NASA TECHNICAL MEMORANDUM

NASA TM X-1682

NASA TM X-1682

EXPERIMENTAL LONGITUDINAL DYNAMICS OF AN EMPTY STUB D ATLAS VEHICLE

by William G. Costakis and Carl F. Lorenzo

Lewis Research Center
Cleveland, Ohio

NATIONAL AERONAUTICS AND SPACE ADMINISTRATION • WASHINGTON, D. C. • NOVEMBER 1968

NASA TM X-1682

EXPERIMENTAL LONGITUDINAL DYNAMICS OF AN EMPTY STUB D ATLAS VEHICLE

By William G. Costakis and Carl F. Lorenzo

Lewis Research Center
Cleveland, Ohio

NATIONAL AERONAUTICS AND SPACE ADMINISTRATION

For sale by the Clearinghouse for Federal Scientific and Technical Information
Springfield, Virginia 22151 – CFSTI price $3.00

ABSTRACT

A test was conducted to determine the longitudinal dynamic characteristics of the Stub D Atlas without propellants or payload. The dynamic characteristics obtained are given in terms of modal damping ratios, vehicle mode shapes, and acceleration responses to a force input over the frequency range of 1 to 120 Hz. Natural frequencies were determined by comparing the acceleration response results with the mode shape and orthogonality test results. The results showed that a one-dimensional model may not be sufficient to predict the behavior of the vehicle.

EXPERIMENTAL LONGITUDINAL DYNAMICS OF AN EMPTY STUB D ATLAS VEHICLE

by William G. Costakis and Carl F. Lorenzo

Lewis Research Center

SUMMARY

A test was conducted to determine the longitudinal dynamic characteristics of the Stub D Atlas without propellants or payload. The dynamic characteristics obtained are given in terms of modal damping ratios, vehicle mode shapes, and acceleration responses to a force input over the frequency range of 1 to 120 hertz. Natural frequencies were determined by comparing the acceleration response results with the mode shape and orthogonality test results. The results showed that a one-dimensional model may not be sufficient to predict the behavior of the vehicle.

INTRODUCTION

A definition of launch vehicle longitudinal dynamics is required in the study of vibrations caused by dynamic coupling between structure, engines, and propellant lines (commonly referred to as POGO) and to determine vehicle structural loads. The dynamic characteristics desired are in terms of modal damping ratios, vehicle mode shapes, and acceleration responses at various vehicle locations to a force input.

An experimental study of the longitudinal dynamics of a Stub D Atlas with water as a simulated propellant, together with the Centaur vehicle and the Surveyor spacecraft as payload, has been reported by Gerus and Housley in reference 1. They also studied the liquid-oxygen-duct inlet pressure response. The experimental results obtained were compared with General Dynamics/Convair's theoretical values. These theoretical values were based on a one-dimensional lumped spring-mass model of the system which treats fluids in the manner described in reference 2. The analysis based on this model predicted natural frequencies reasonably well but did not predict the amplitude of the pressure oscillations at the liquid-oxygen-duct inlet (tank base) with adequate accuracy. This pressure is one of the key factors in the analysis of the POGO oscillations.

From the results of reference 1, it was evident that an improvement of the present one-dimensional model of the vehicle was in order. Before this problem can be attacked, a better description of the empty Atlas dynamic response and its contribution to the overall damping is needed (ref. 3). This investigation was conducted to determine the longitudinal dynamic characteristics of a Stub D Atlas vehicle without payload or propellants.

TEST APPARATUS AND PROCEDURE

Test Vehicle

The test vehicle employed was a Stub D Atlas S/N 116 with a Centaur interstage adapter attached. A stiffening ring was added to the top of the interstage adapter to allow attachment of lateral stabilization springs.

The booster and sustainer engines of the vehicle were removed and replaced with an equivalent-weight X-frame which served also as anchor points for the suspension system (fig. 1). The X-frame mass was 5400 pounds mass (2449 kg) and was considered to be rigid over the frequency range of interest.

During all tests, the Atlas was maintained at standby pressures of 8 and 16 psig (5.516×10^4 and 11.032×10^4 N/m^2 gage) for the liquid-oxygen and fuel tanks, respectively. The tanks contained no liquids. These pressures were chosen so that personnel could enter the testing area during testing without risk.

Suspension System

The vehicle was supported during the dynamic tests by a suspension system (fig. 1) which consisted of a rigid frame at the base of the vehicle (X-frame) suspended by four steel cables, each of which was in turn suspended by a spring box containing 16 springs each (fig. 2). The spring boxes were, in turn, connected to the tower structure through a lifting and vehicle-weight-measuring system.

Lateral stability was provided by a set of four radial springs attached to the stiffening ring at the top of the interstage adapter and a set of eight tangential springs on the X-frame. The spring rates and arrangements are shown in figures 3 and 4.

Force input to the Atlas was effected at the booster engine attachment points on the vehicle y-axis. The vehicle also contacted the X-frame at the x-axis; however, these points served only to stabilize the vehicle and, hence, carried only a small part of the total weight.

The suspension system spring constant was chosen so that the rigid-body mode

would be within the measurable frequency range. The total stiffness of the suspension system was set (by using 16 springs per box) at 25 866 pounds per inch (4.530×10^6 N/m). The effective stiffness, however, was calculated from the observed natural frequency at 20 500 pounds per inch (3.590×10^6 N/m). This was so because a number of individual springs were not always engaged due to variations in the unloaded spring lengths. The exciter flexures had a stiffness (in the axial direction) of 7000 pounds per inch (1.226×10^6 N/m), which becomes part of the suspension system stiffness during logarithmic decay.

Instumentation

Three basic types of measurements were made: skin accelerations, force input from the exciter, and displacements.

Piezoelectric-type accelerometers were used for all but the low-frequency ($f < 10$ Hz) testing. The accelerometers were mounted on small plastic cubes which were in turn glued to the vehicle skin (fig. 5). All accelerometers were mounted on the skin of the vehicle so as to detect longitudinal motion. Twenty-eight accelerometers were mounted on the +x-axis side and six on the +y-axis side of the vehicle, as shown in figure 6.

Exciter force input to the X-frame was measured with a strain-type 15 000-pound (6.672×10^4-N) load cell mounted between the exciter and the X-frame (see fig. 7). The piezoelectric-type accelerometer and load cell measurement accuracies were estimated to be better then 4 percent and 1 percent of full scale, respectively.

For the low-frequency testing ($f < 10$ Hz) of the vehicle suspension system, linear potentiometers were used to indicate X-frame and interstage adapter position. At these frequencies, the linear potentiometers exhibited no dynamic degradation. Also, ten strain-gage-type accelerometers, with flat low-frequency response, were distributed over the vehicle, as shown in figure 8.

The vehicle was driven along the longitudinal axis by an electrodynamic shaker through the load cell and the X-frame (fig. 9). The suspension system was used to counteract the weight of the vehicle and, thus, allow the shaker to supply only the dynamic part of the force. For high frequency ($f > 10$ Hz), the shaker current was supplied by an electronic amplifier. The test procedure for high frequency was simply to drive the system at the frequency of interest until sinusoidal steady-state was achieved and record a suitable sample of the instrument response through a digitizer system. For all sinusoidal tests, the driving force was adjusted so that the acceleration never exceeded 1 g (9.807 m/sec^2) on the vehicle or $\pm 1/4$-inch (0.635×10^{-2}-m) displacement of the X-frame. Generally, acceleration amplitude was kept at the 3/4-g (7.355-m/sec^2) level. Under these conditions, the force levels ranged from 2000 to 13 000 pounds (8.896×10^3 to 57.827×10^3 N).

The test procedure to determine the vehicle suspension system characteristics at low

frequency varied from that at high frequency in that an amplidyne was used to supply exciter current.

To find the damping of a given mode, the system was driven at the modal frequency until sinusoidal steady-state was achieved. The shaker power was then cut off and the decay of a representative set of vehicle accelerations at 12 vehicle positions was recorded on magnetic tape (analog signals). The damping ratios were then determined by using the logarithmic decay technique.

TEST RESULTS AND DISCUSSION

The magnitude and phase angle of the acceleration relative to force of 28 positions on the +x-axis side and 6 positions on the +y-axis side of the vehicle are plotted against frequency and presented in figures 10 and 11.

These responses were obtained from the steady-state sinusoidal tests. The frequency range was from 1 to 120 hertz. The acceleration-relative-to-force plots presented herein show the response from 10 to 120 hertz. These plots show a great number of resonances, but the most predominant are at 19, 40, 47, 72, 78, and 117 hertz. The response of the displacement relative to force of the X-frame is plotted against frequency in the 1- to 12.5-hertz range (fig. 12). The suspension system vehicle mode (rigid-body mode) for the system occurred at 3.5 hertz.

Other than the rigid-body natural frequency, the determination of the natural frequencies from the plots of amplitude ratio against frequency proved to be a rather difficult task because of the number of resonances that were observed. For this reason, vehicle dynamic shape plots of acceleration magnitude and phase angle relative to force, both against station, were obtained for a number of frequencies (fig. 13). These plots show that the longitudinal responses of all stations were nearly in phase at the lower frequencies (relative to 47 Hz). As the frequencies increased, the phase gradually shifted until, at 47 hertz, there was a 180° phase shift from the base of the vehicle to the top. This indicates that the resonances which occurred below 47 hertz were oriented in other planes and may have been coupled, lateral, or shell resonances. From these considerations, it may be concluded that 47 hertz is the first vehicle longitudinal mode.

Orthogonality tests were conducted for a number of resonance points and the results are presented in table I. The normalized orthogonality condition is given by

$$\frac{\int_0^{\ell} W(z)\left(\frac{\ddot{u}_n(z)}{F}\right)\left(\frac{\ddot{u}_m(z)}{F}\right) dz}{\sqrt{\int_0^{\ell} W(z)\left(\frac{\ddot{u}_n(z)}{F}\right)^2 dz}\sqrt{\int_0^{\ell} W(z)\left(\frac{\ddot{u}_m(z)}{F}\right)^2 dz}} = \begin{cases} 0 & \text{for } n \neq m \\ 1 & \text{for } n = m \end{cases}$$

where ℓ is the length of the vehicle, W(z) is the mass per unit length of the vehicle, and $\ddot{u}_n(z)/F$ and $\ddot{u}_m(z)/F$ are the dynamic shapes of the vehicle at resonant test frequencies n and m. This type of orthogonality normalization is given in reference 4. The integrals were numerically evaluated using Gauss' quadrature method.

In order to apply the orthogonality condition, the following assumptions are made:

(1) The effect of vehicle damping was negligible.

(2) Since the first accelerometer was at station 548 and not at the top of the vehicle (station 413), the weight of the vehicle from stations 413 to 548 was considered to be part of the weight of the first summation increment.

(3) The X-frame was assumed to be rigid. Therefore, the bottom of the X-frame (station 1278) has the same dynamic response as the top (station 1254).

The orthogonality expression was evaluated by using the digital computer. The least-squares method was used in curve fitting the dynamic shapes from known data points. A plot of vehicle mass distribution against distance is presented in figure 14.

The near orthogonality between the 3.5- and 47-hertz modes indicates that 47 hertz is the first vehicle longitudinal mode. This agrees with the mode-shape and phase-angle-against-station results. The results also showed that the 92.8-hertz mode was orthogonal to the 47-hertz mode but was not orthogonal to the 3.5-hertz mode.

The amplitude ratio plots showed rather large resonance at 72, 78, and 117 hertz. The vehicle dynamic plots show that the phase angle at 72 and 78 hertz shifts through 285° and 305°, respectively, in comparison to 360° for a second flexible mode, while it is inconclusive at 117 hertz. The phase angle at 110 hertz, however, shifts through 540°, which is characteristic of the third flexible mode, indicating that the 117-hertz resonance is beyond the range of the second mode. The orthogonality test results did not show either the 72- or the 78-hertz resonance as orthogonal to the 3.5- and 47-hertz modes.

The y-axis side results for stations 572, 596, 764, and 932 (figs. 11(a) to (d)) match their respective x-axis results (figs. 10(b), (c), (e), and (h)) in both amplitude and phase angle. The y-axis side results for stations 1148 and 1176 (figs. 11(e) and (f)) do not match their respective x-axis side results (figs. 10(n) and (o)) at all frequencies.

For stations 1148 and 1176, the amplitude ratio on the y-axis side at 47.5 hertz was larger than the x-axis side amplitude ratio by factors of 2.80 and 2.20, respectively. At higher frequencies, the reverse was true; x-axis values exceeded y-axis values at 78, 83,

and 92.5 hertz by an average factor of 1.95, 1.74, and 1.21, respectively. The phase angle was different between the two sides from 36 to 70 hertz and from 100 to 120 hertz. This difference indicates that the dynamic characteristics are the same for the upper portion of the vehicle for both x- and y-axis sides but are not the same for the lower portion. This can be attributed to the fact that the upper portion of the vehicle is symmetrical while the lower portion is not. The asymmetry is caused by the long and short pods attached to the skin of the vehicle on the -y and +y sides, respectively.

Damping was calculated by using the logarithmic decay method, the damping ratio ζ given by

$$\zeta = \frac{1}{2\pi N} \ln \frac{A_o}{A_N}$$

where ζ is the ratio of the actual damping to the critical damping and A_o and A_N are the amplitudes at the zero and N^{th} cycles of the decaying sinusoidal wave. The damping associated with the suspension system was 5 percent of critical based on logarithmic decay and 4.6 percent of critical based on the peak value of the amplitude. The damping values at 47 and 72 hertz were 1.6 and 1.45 percent of critical, respectively, based on logarithmic decay. These modal damping constants are functions of the vehicle and suspension system local damping. The suspension system damping, in particular, can greatly influence the first flexible mode damping even though the frequencies are well separated. The relative magnitude of this effect can be determined by the methods of reference 3. Some of the modal frequencies, percentages of critical damping, and their respective transient decay plots are shown in figure 15.

CONCLUDING REMARKS

From the study of the orthogonality test results, vehicle dynamic shapes, and frequency responses, we can reasonably conclude that the rigid-body mode of the vehicle and suspension system is at 3.5 hertz and the first vehicle longitudinal flexible mode is at 47 hertz. From the amplitude ratio results and the vehicle dynamic shapes the 78-hertz, or possibly the 72-hertz, mode might be considered to be the second flexible mode. However, this possibility could not be substantiated by orthogonality results. Damping at these modes, using the logarithmic decay method, was 5.0, 1.6, and 1.45 percent of critical, respectively.

Since results for the x-axis and y-axis sides compare extremely well for stations 572 to 932, it can be concluded that the dynamic characteristics of the upper portion of the vehicle are the same for both sides over the test frequency range.

For the lower portion of the vehicle, the x- and y-axis results did not match, which means that the dynamic characteristics there are not the same for both sides. This is so because the vehicle is asymmetrical at the lower portion. In the upper part of the vehicle where the results matched, the vehicle is symmetrical.

Because of the number of resonances shown in the acceleration response results, a one-dimensional spring-mass model may not be sufficient to predict the behavior of the vehicle. The apparent coupling of modes and the number of resonances indicates that more refined models incorporating bending and shell effects might be necessary for empty and near-empty conditions.

Lewis Research Center,
National Aeronautics and Space Administration,
Cleveland, Ohio, May 9, 1968,
180-31-01-01-22.

APPENDIX - SYMBOLS

A	amplitude of sinusoidal wave
F	applied force, lb (N)
f	frequency, Hz
l	length of vehicle, in. (m)
u	longitudinal displacement, in. (m)
$\ddot{u}$	longitudinal acceleration, g (m/sec^2)
W	mass per unit length of the vehicle, mass/in. (kg/m)
x	horizontal direction as shown in fig. 6
y	horizontal direction as shown in fig. 6
z	vertical direction
ζ	ratio of actual damping to critical damping

REFERENCES

1. Gerus, Theodore F.; Housley, John A.; and Kusic, George: Atlas/Centaur/Surveyor Longitudinal Dynamics Test. NASA TM X-1459, 1967.

2. Wood, John D.: Survey on Missile Structural Dynamics. STL 7102-0041-NU-000, EM 11-11 (BSD-TN-61-42), Space Technology Labs., Inc., June 1, 1961.

3. Koenig, Harry J.; and Drain, Daniel I.: Method of Relating Modal Damping to Local Dampers in Lumped-Parameter Systems. NASA TN D-3637, 1966.

4. Keith, J. S.: Methods in Structural Dynamics for Thin Shell Clustered Launch Vehicles. Ling-Ternco-Vought, Inc. (FDL-TDR-64-105, DDC No. AD-463571), Apr. 1965, p. 37.

TABLE I. - ORTHOGONALITY TEST RESULTS

Frequency, Hz	3.4977	19.206	40.903	46.725	46.950	53.437	71.803	78.755	92.774
3.4977	1	0.997	0.553	0.039	0.026	0.119	-0.635	-0.541	-0.564
19.206		1	.588	.0857	.0719	.179	-.582	-.489	-.521
40.903			1	.851	.845	.836	.161	-.122	-.242
46.725				1	.999	.936	.602	.206	.071
46.950					1	.931	.601	.196	.061
53.437						1	.644	.391	.238
71.803							1	.847	.768
78.755								1	.959
92.774									1

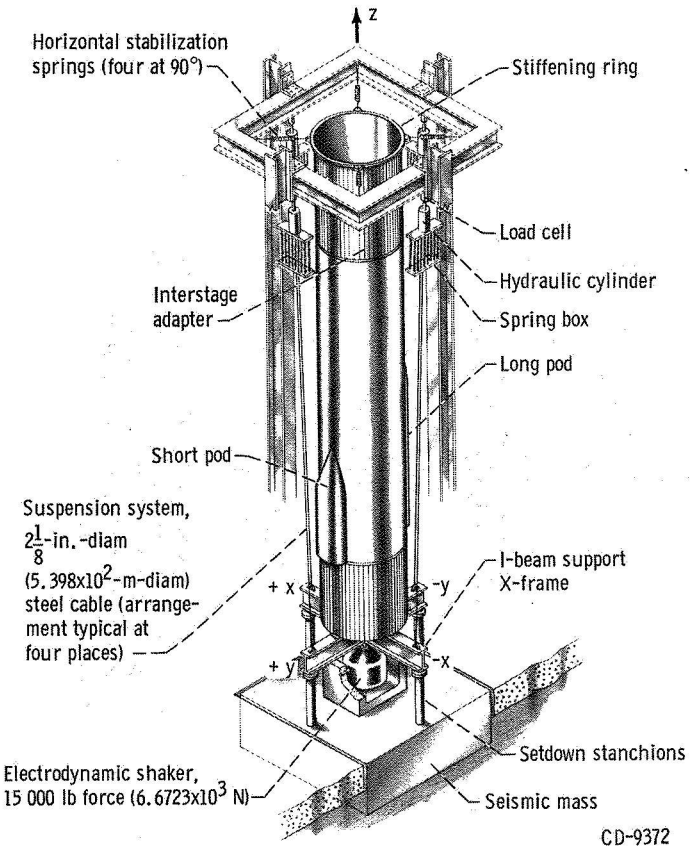

Figure 1. - Vehicle support system.

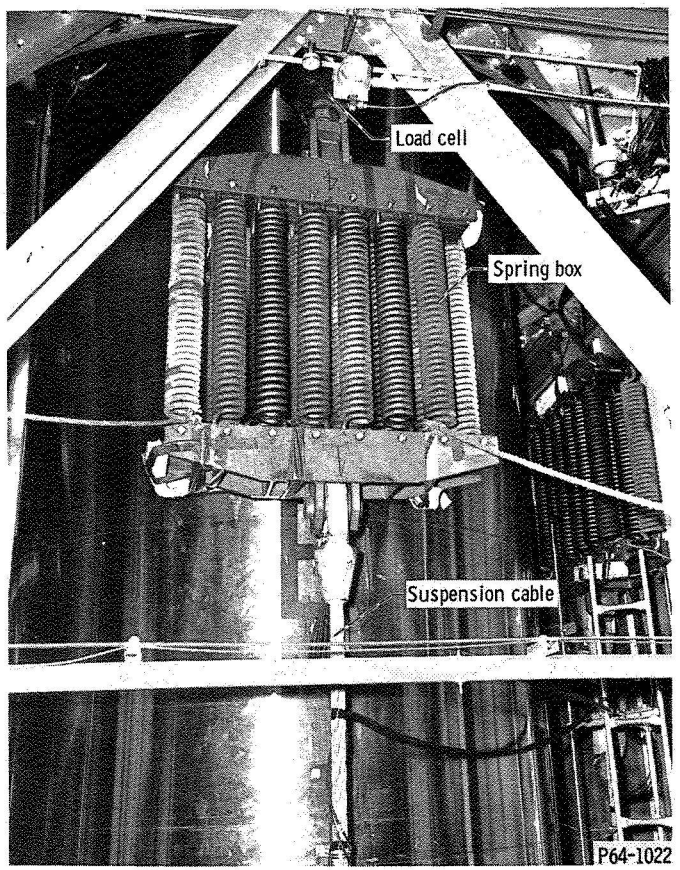

Figure 2. - Closeup of suspension springs.

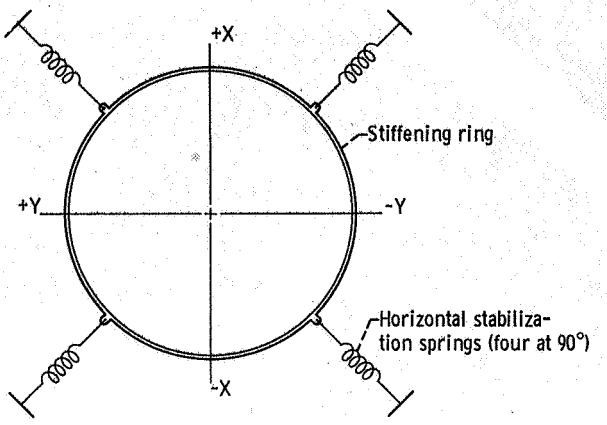

Figure 3. - Stabilization system, four radial springs attached to stiffening ring. (The spring rate of each spring is 300 lb/in. (5.254×10^4 N/m). Each spring was stretched to 100 lb (4.448×10^2 N), ±5 percent.)

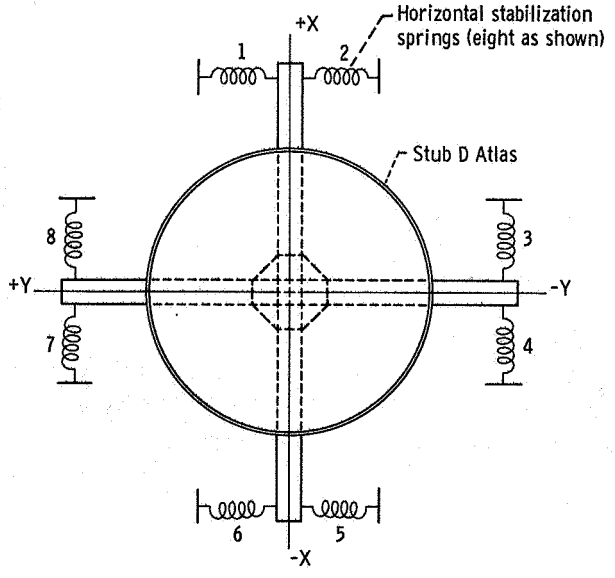

Figure 4. - Stabilization system, a set of eight tangential springs attached to X-frame. (Springs 1, 2, 5, and 6 have a spring rate of 200 lb/in. (3.503×10^4 N/m); springs 3, 4, 7, and 8 have a spring rate of 100 lb/in. (1.751×10^4 N/m). Each spring was stretched to 100 lb (4.448×10^2 N), ±10 percent.)

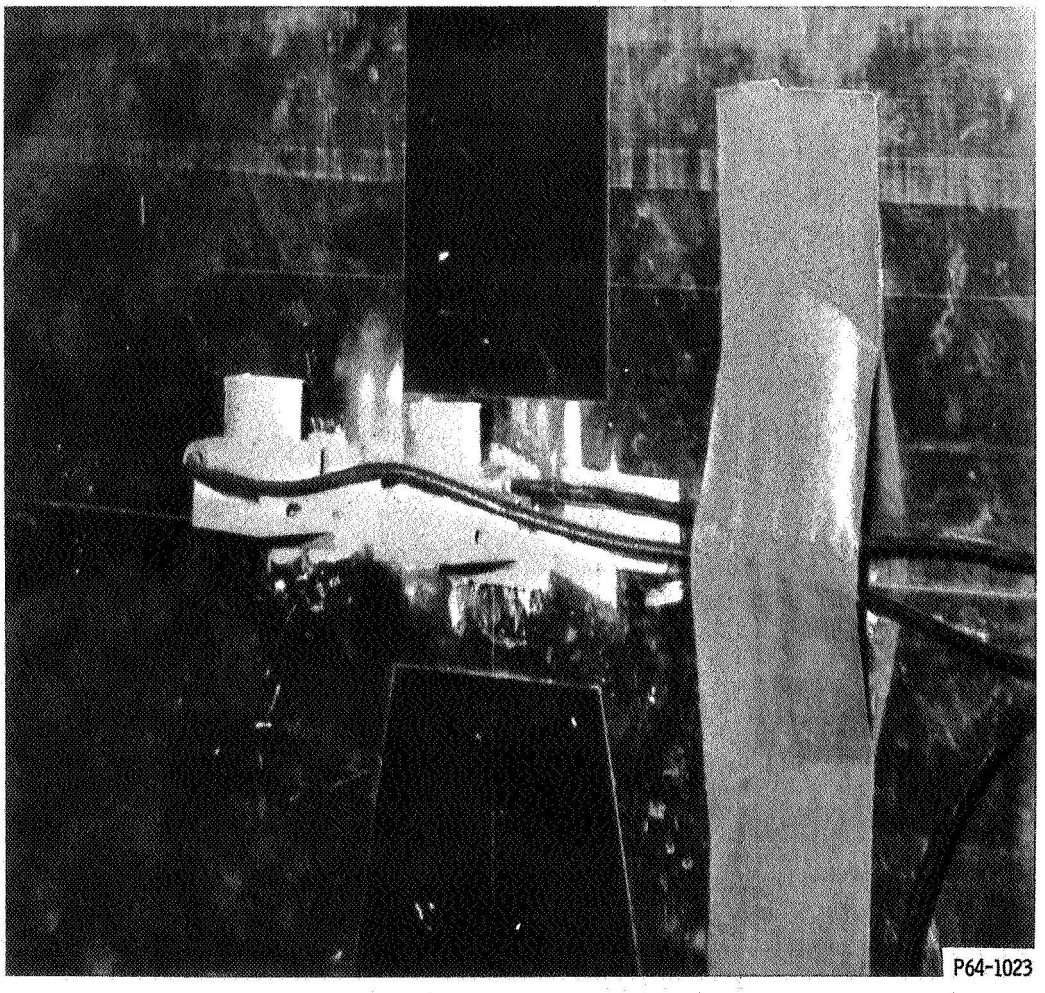

Figure 5. - Typical mounting of piezoelectric-type accelerometers.

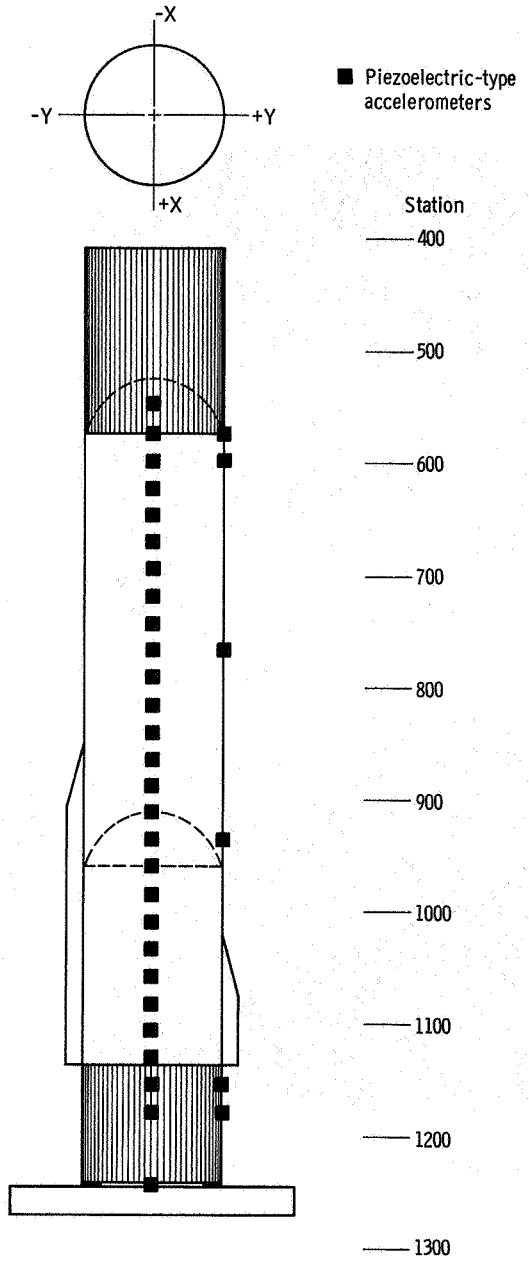

Figure 6. - Instrument location for longitudinal dynamics tests.

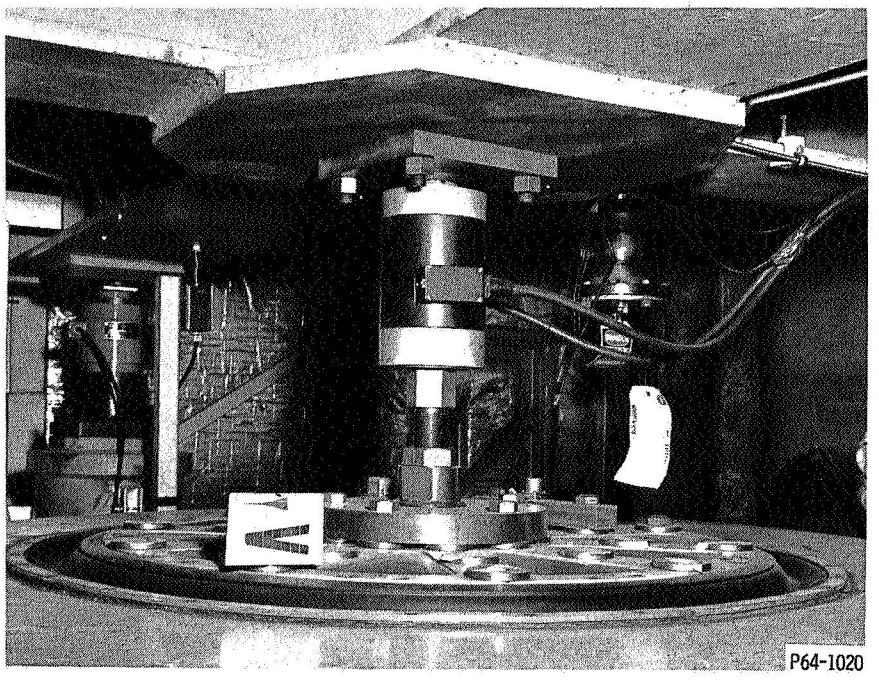

Figure 7. - Mounting of load cell.

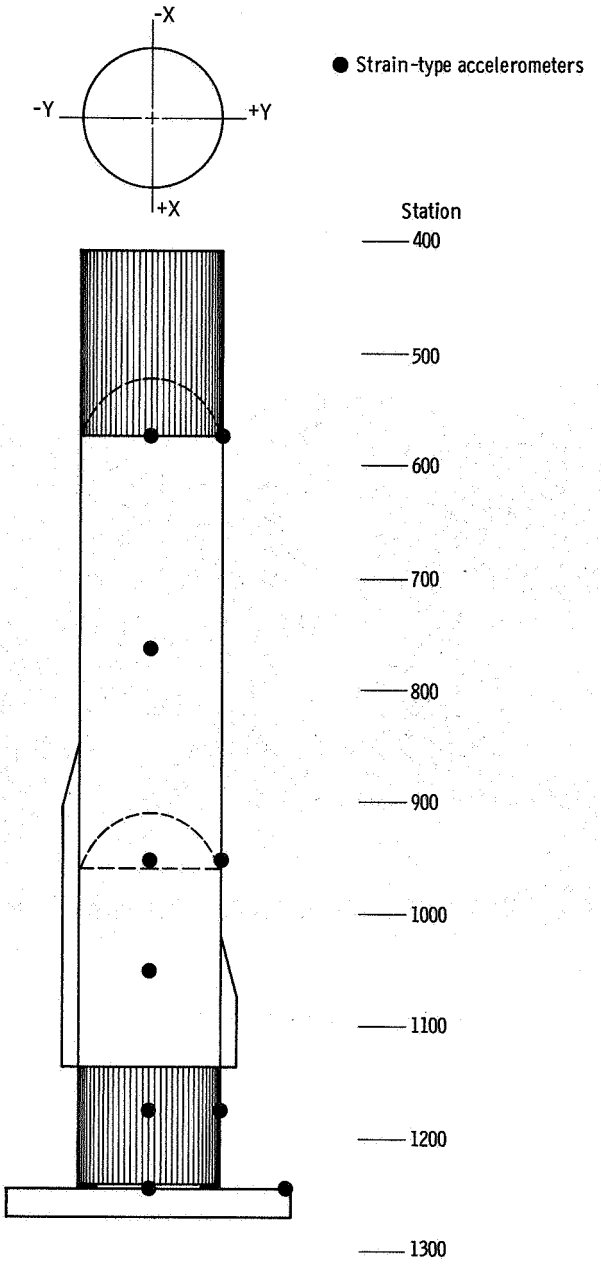

Figure 8. - Location of additional instrumentation for low-frequency tests.

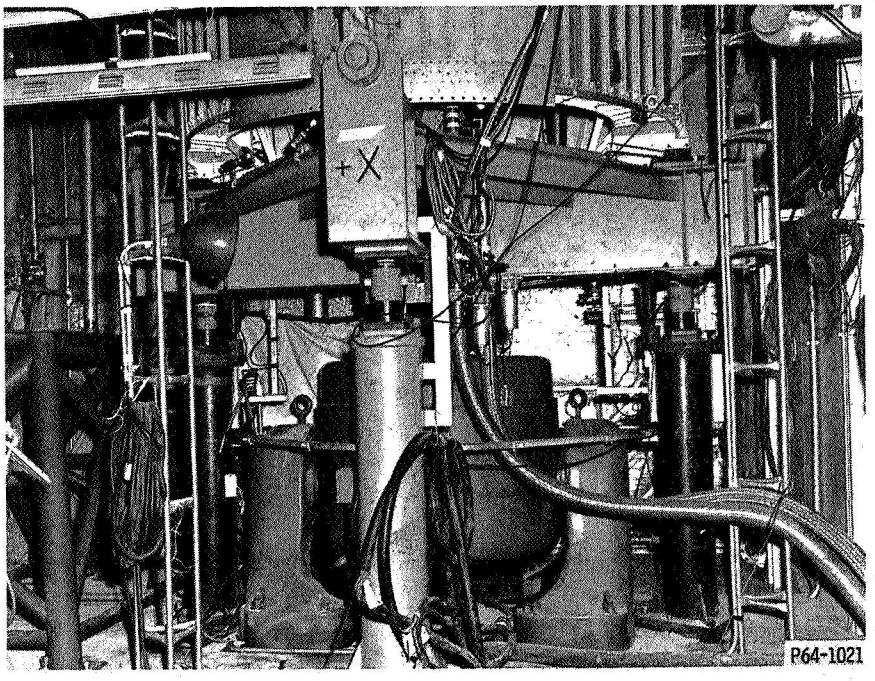

Figure 9. - Electromagnetic shaker and X-frame.

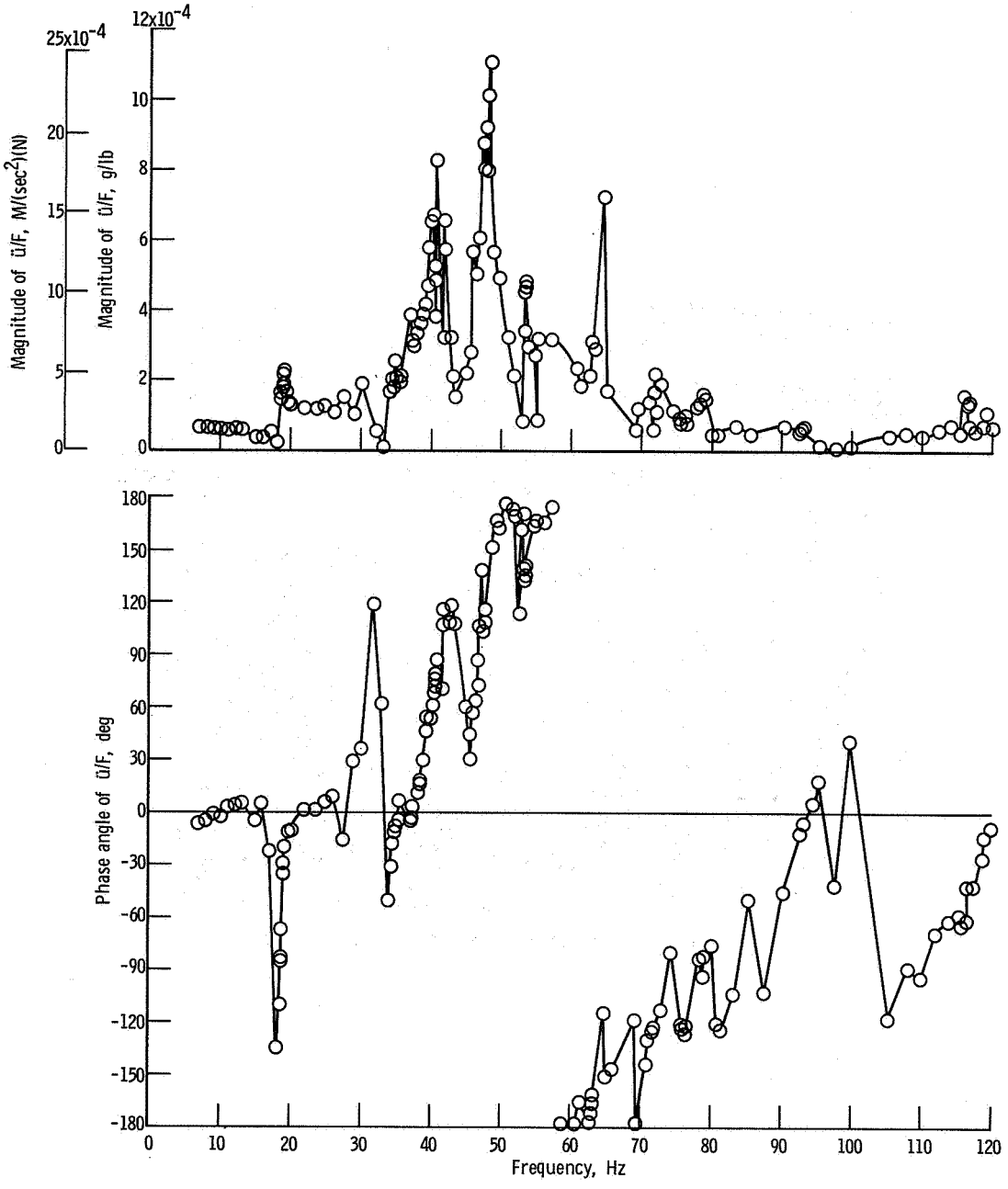

(a) Station 548.

Figure 10. - Longitudinal dynamic response of the vehicle side oriented in the +x-axis direction.

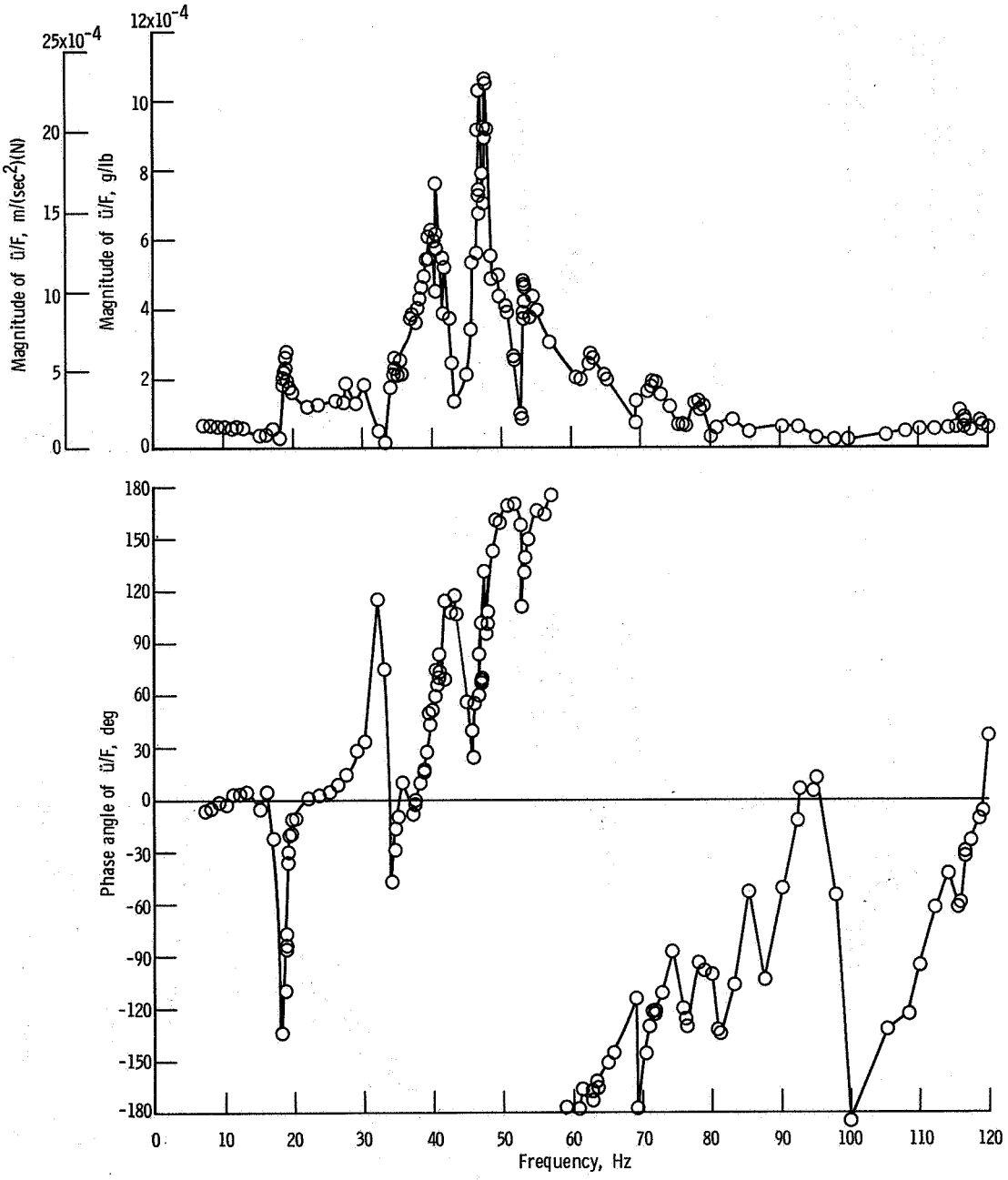

(b) Station 572.

Figure 10. - Continued.

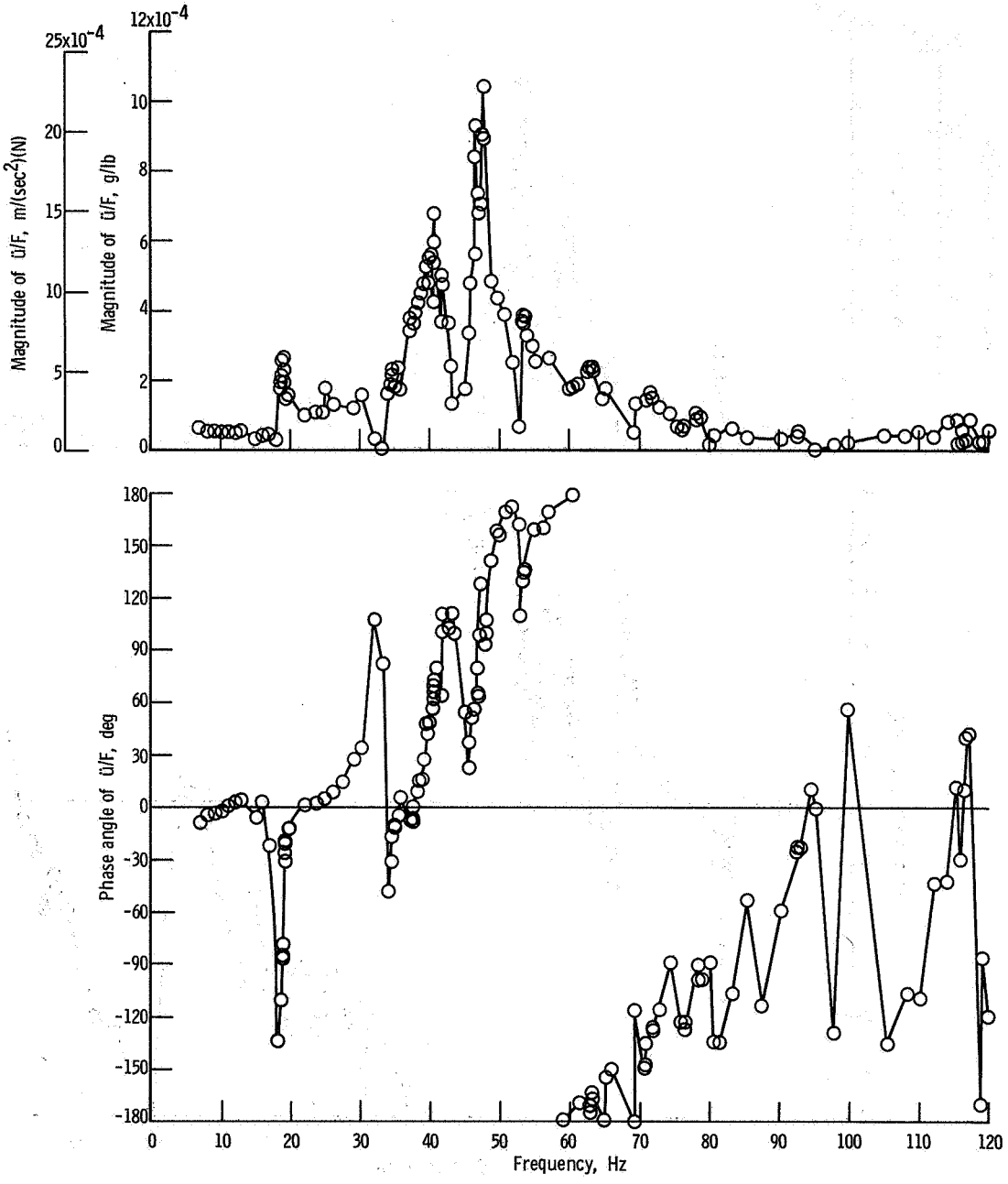

(c) Station 596.

Figure 10. - Continued.

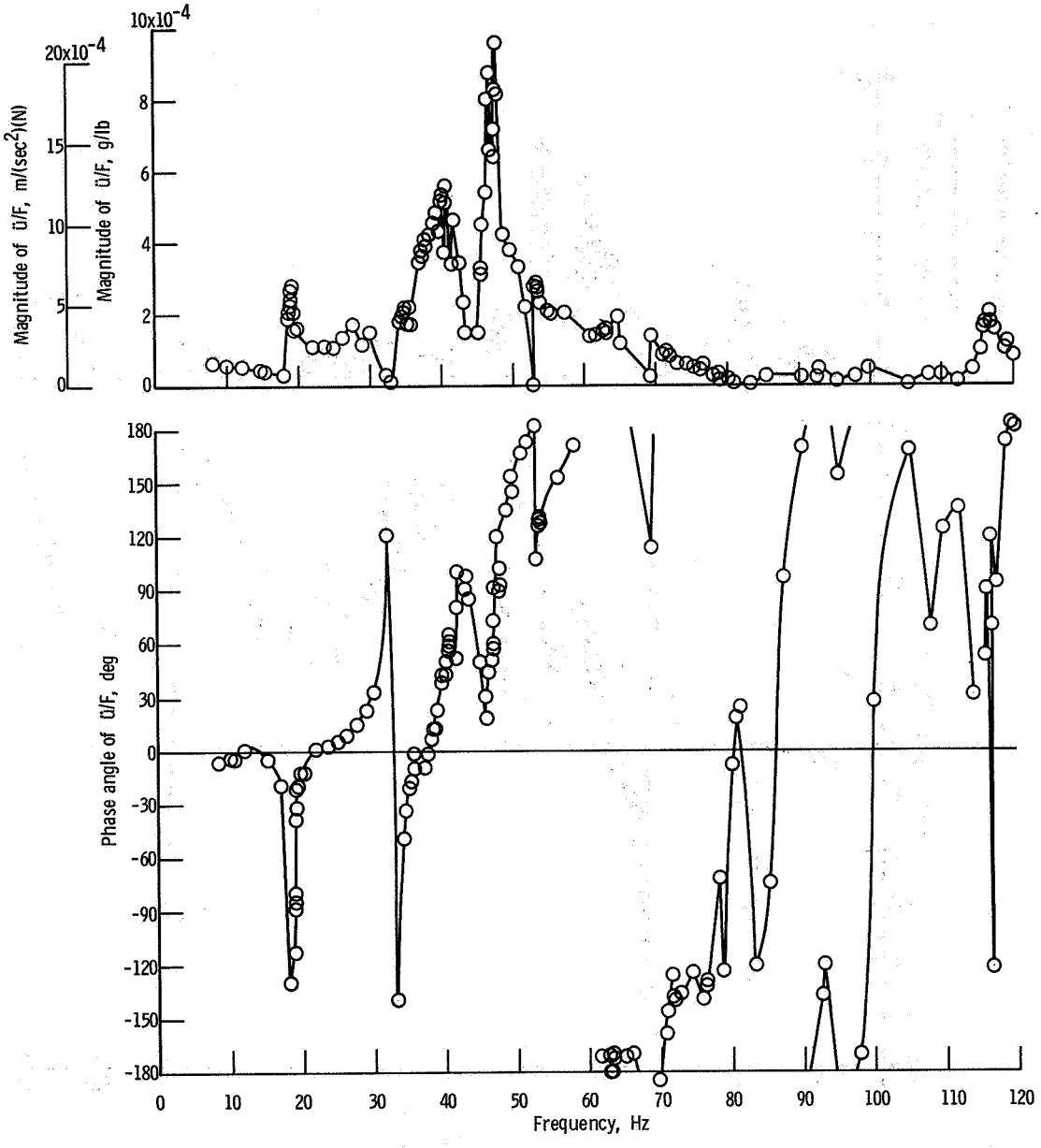

(d) Station 668.

Figure 10. - Continued.

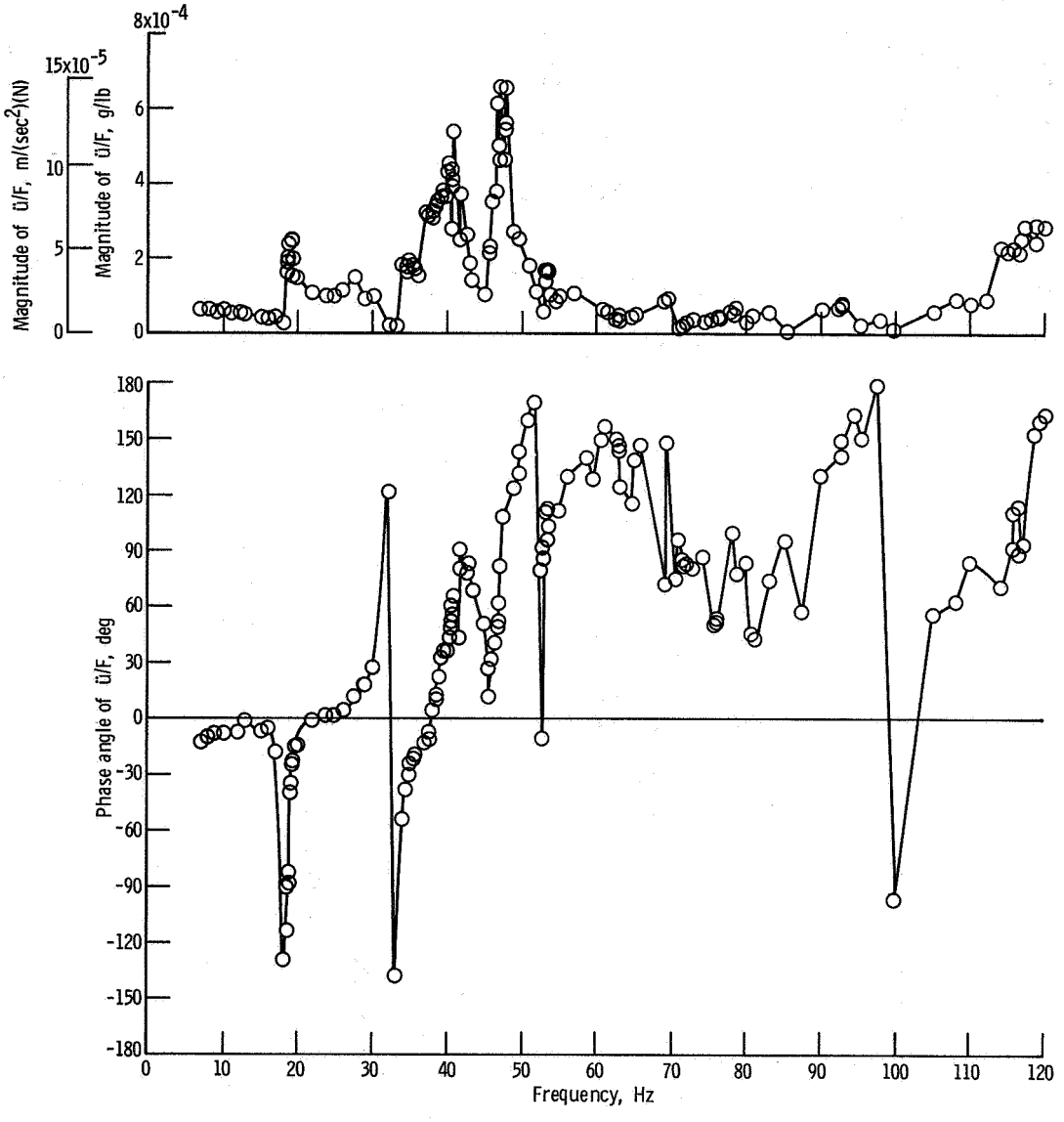

(e) Station 764.

Figure 10. - Continued

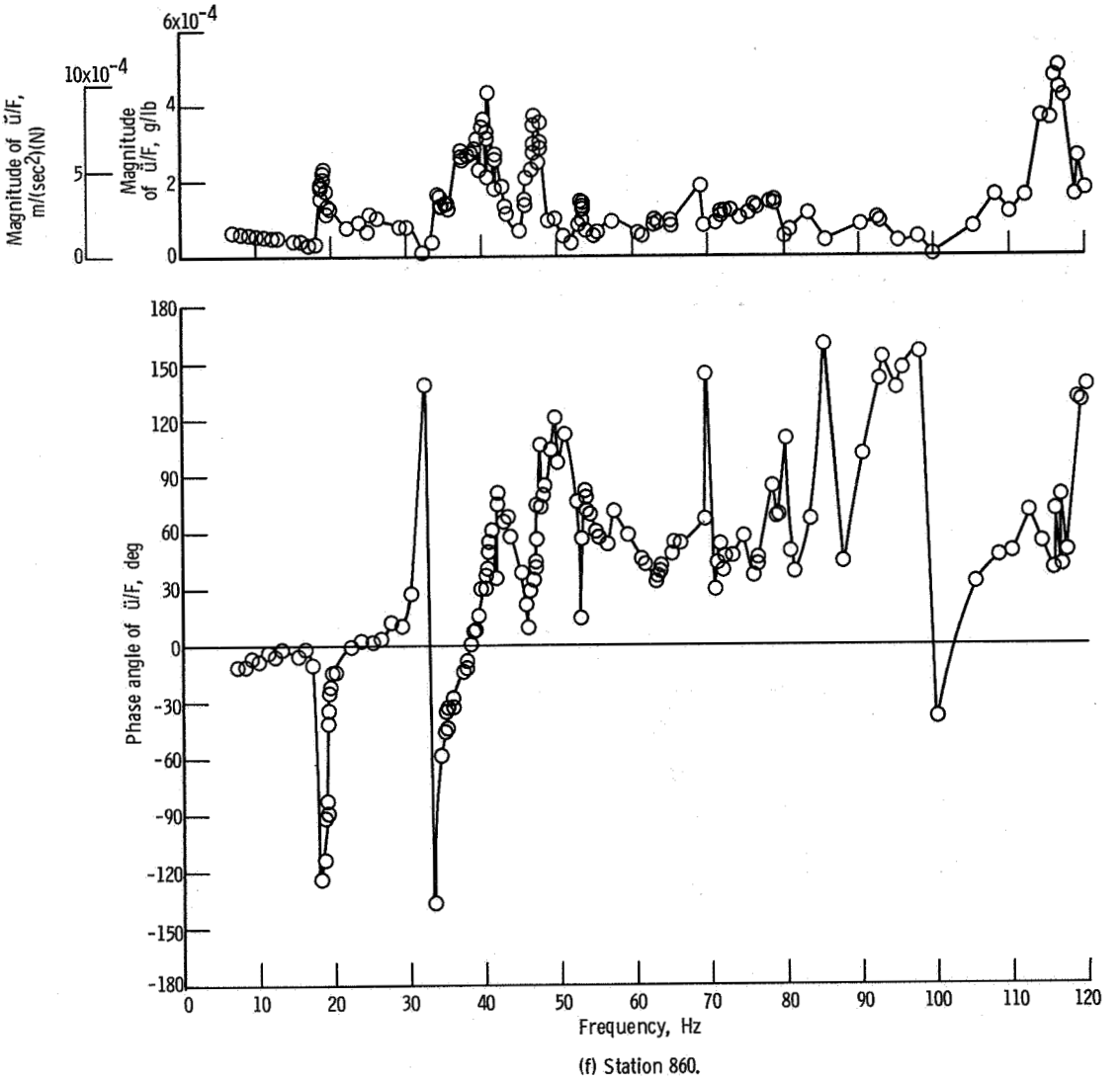

(f) Station 860.

Figure 10. - Continued

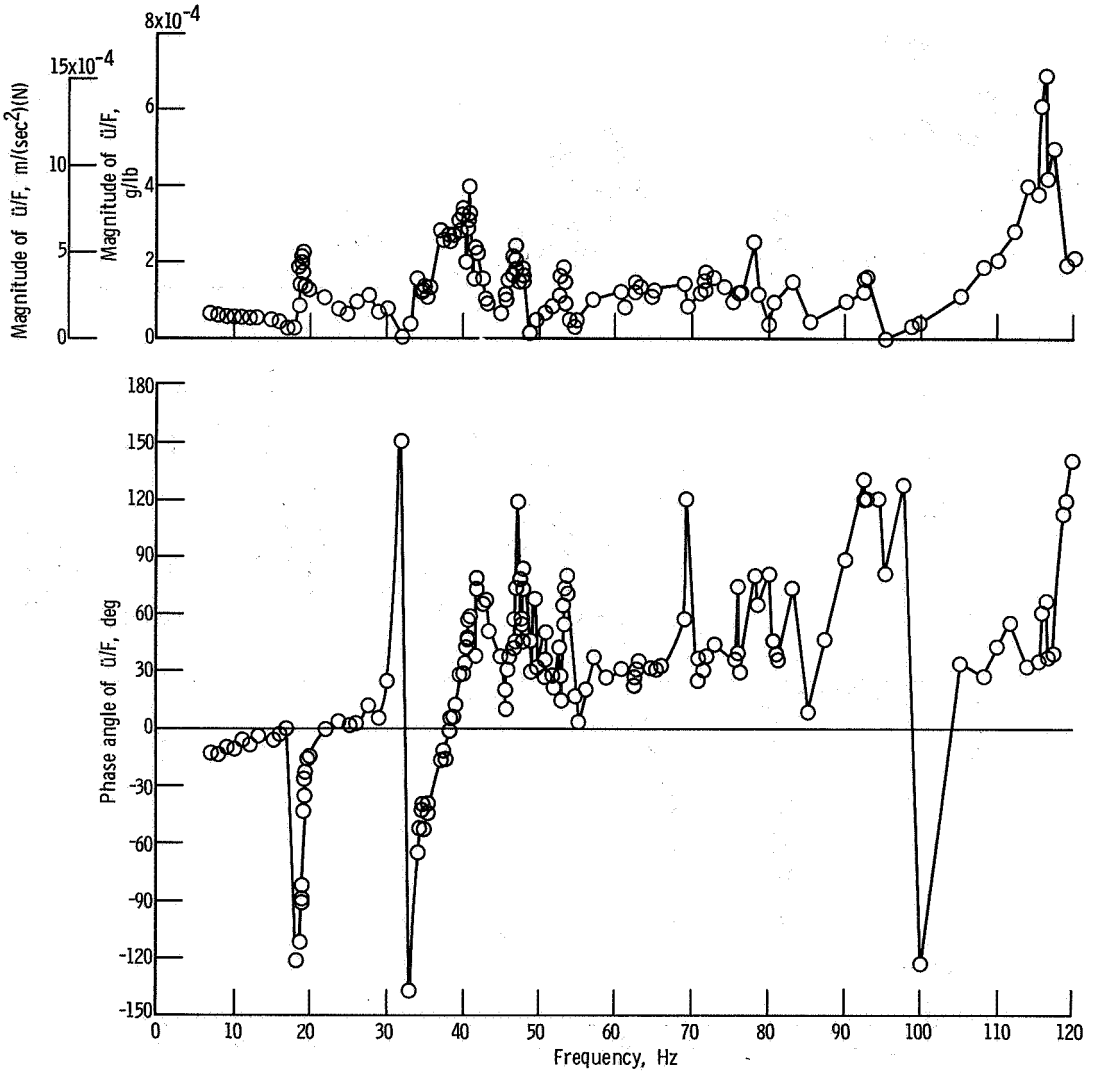

(g) Station 908.

Figure 10. - Continued.

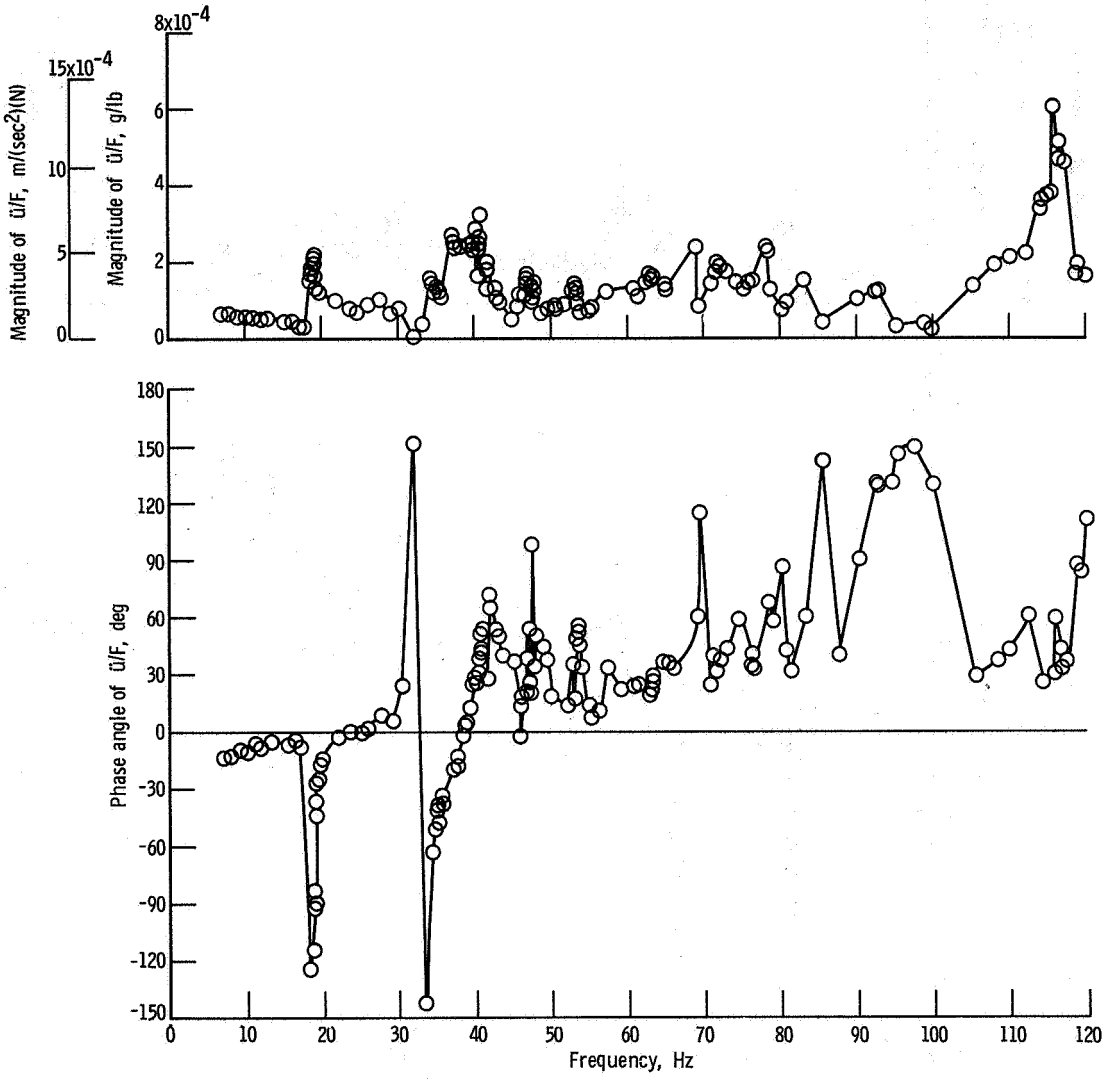

(h) Station 932.

Figure 10. - Continued.

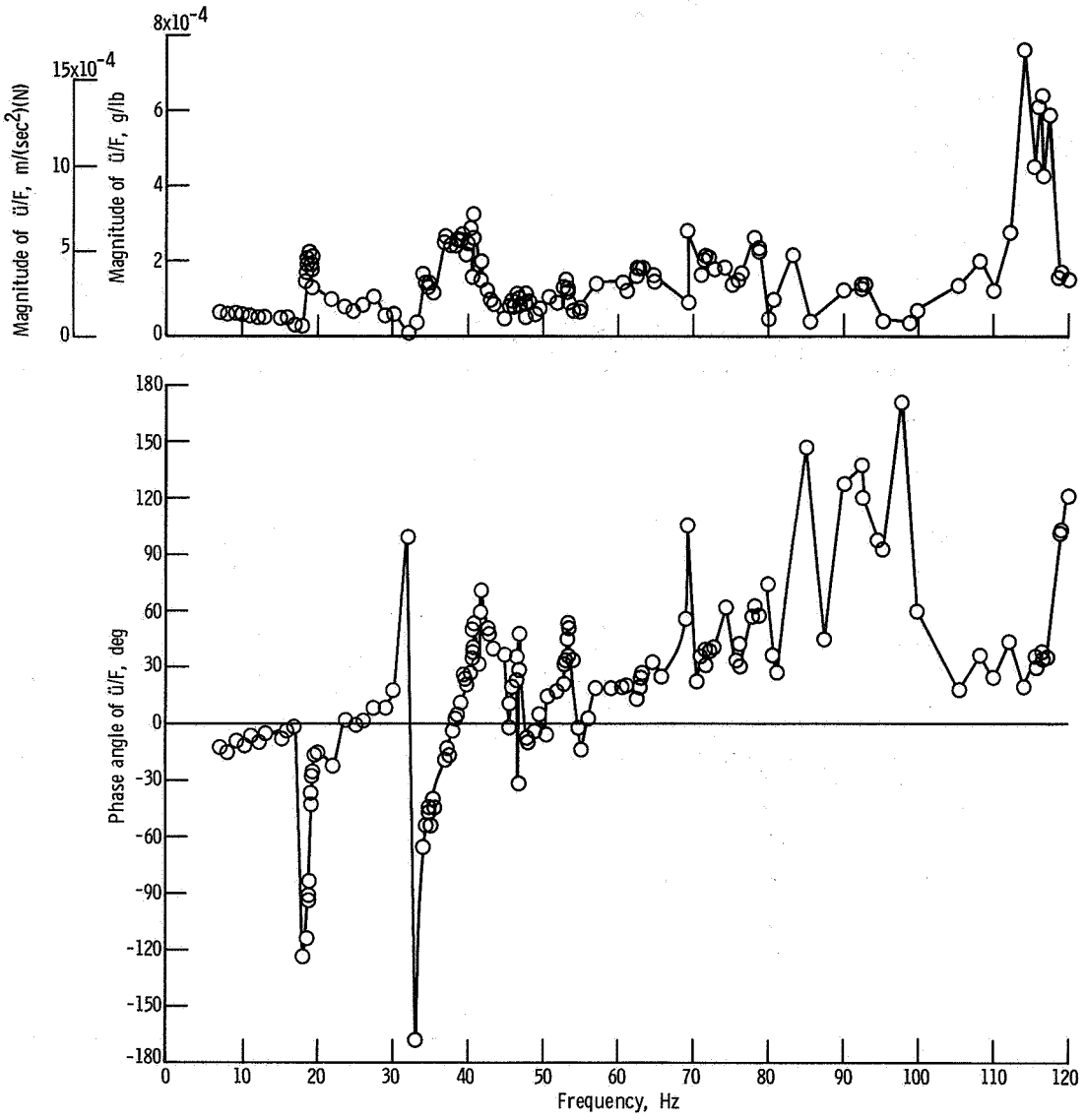

(i) Station 956.

Figure 10. - Continued.

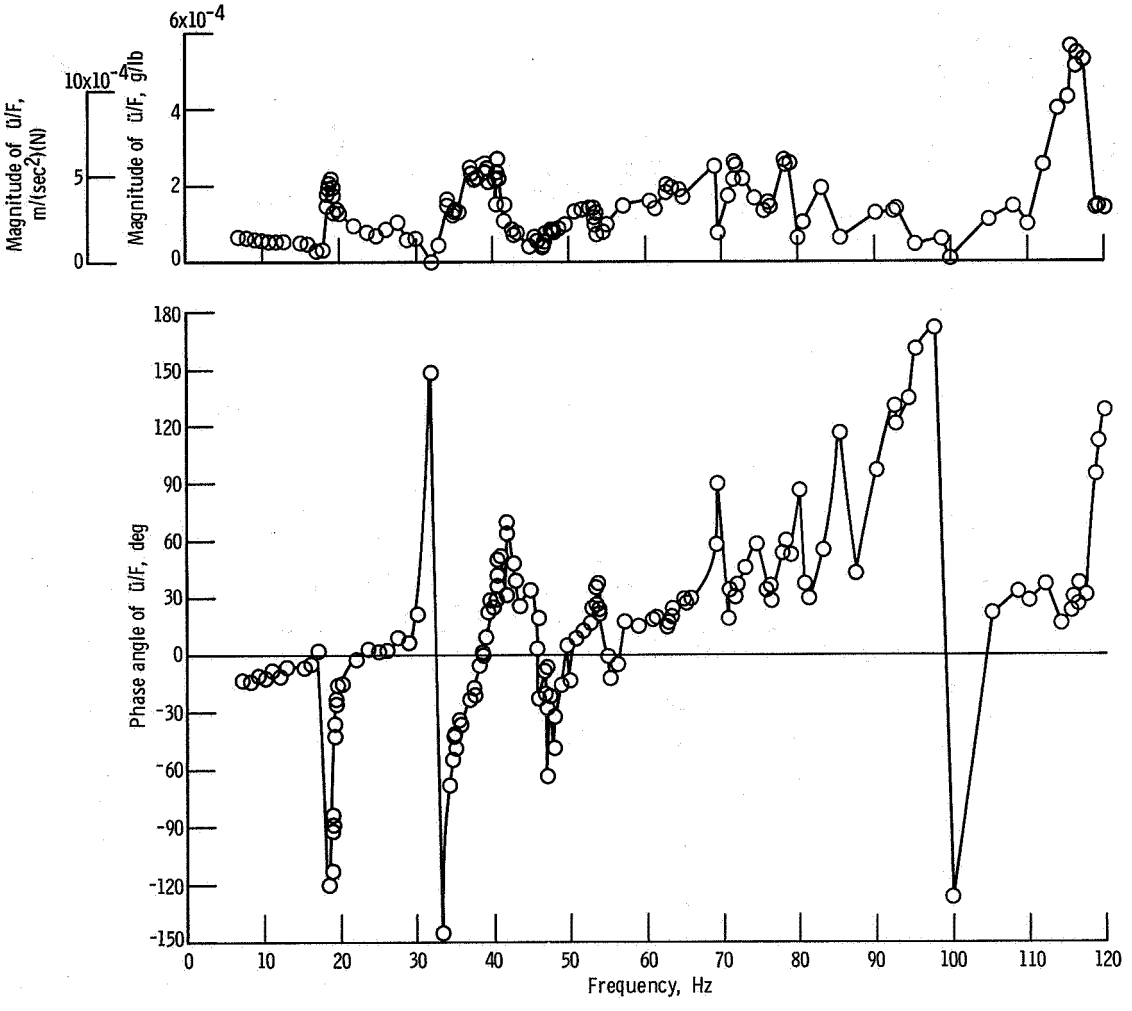

(j) Station 980.

Figure 10. - Continued.

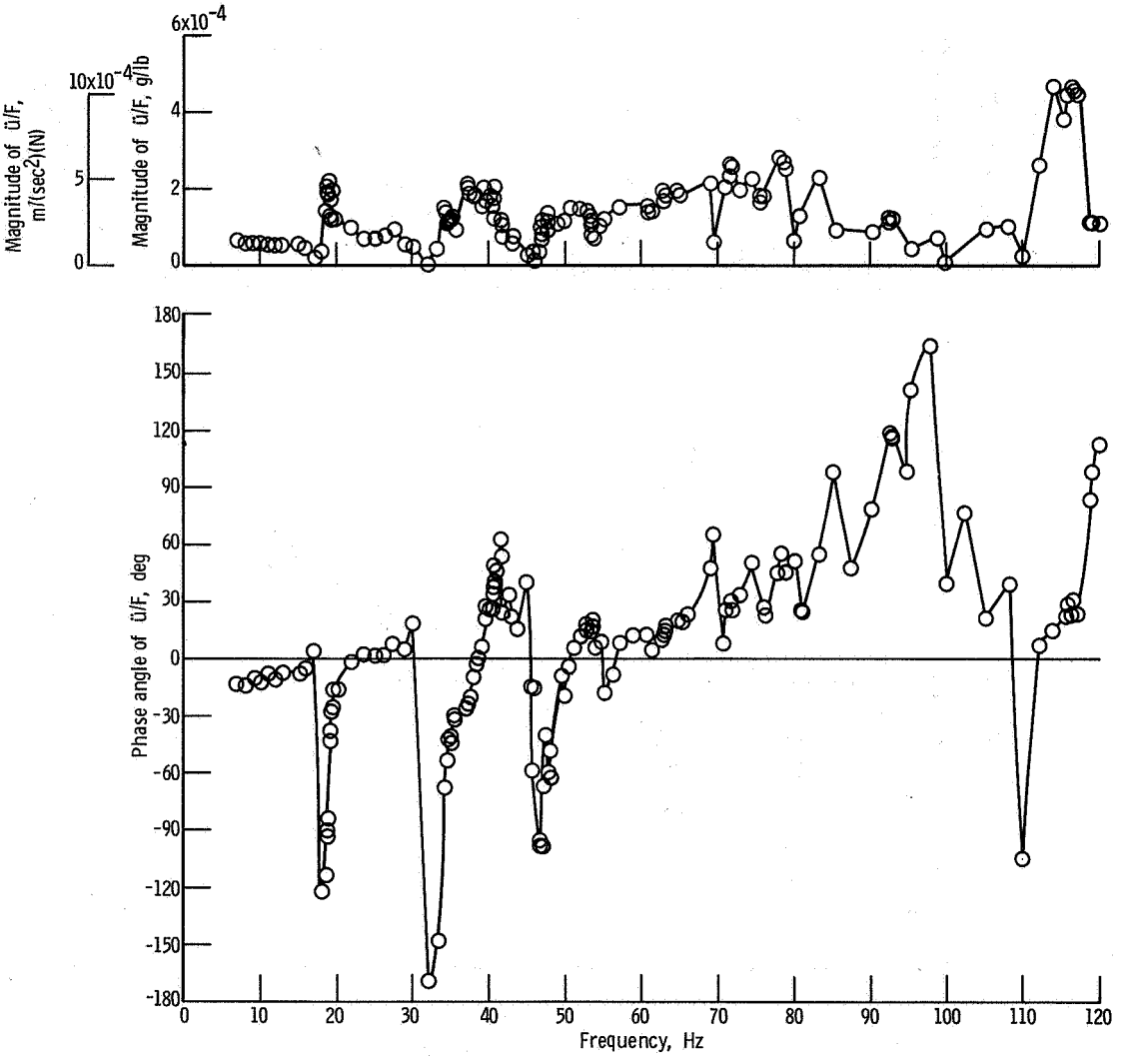

(k) Station 1028.

Figure 10. - Continued.

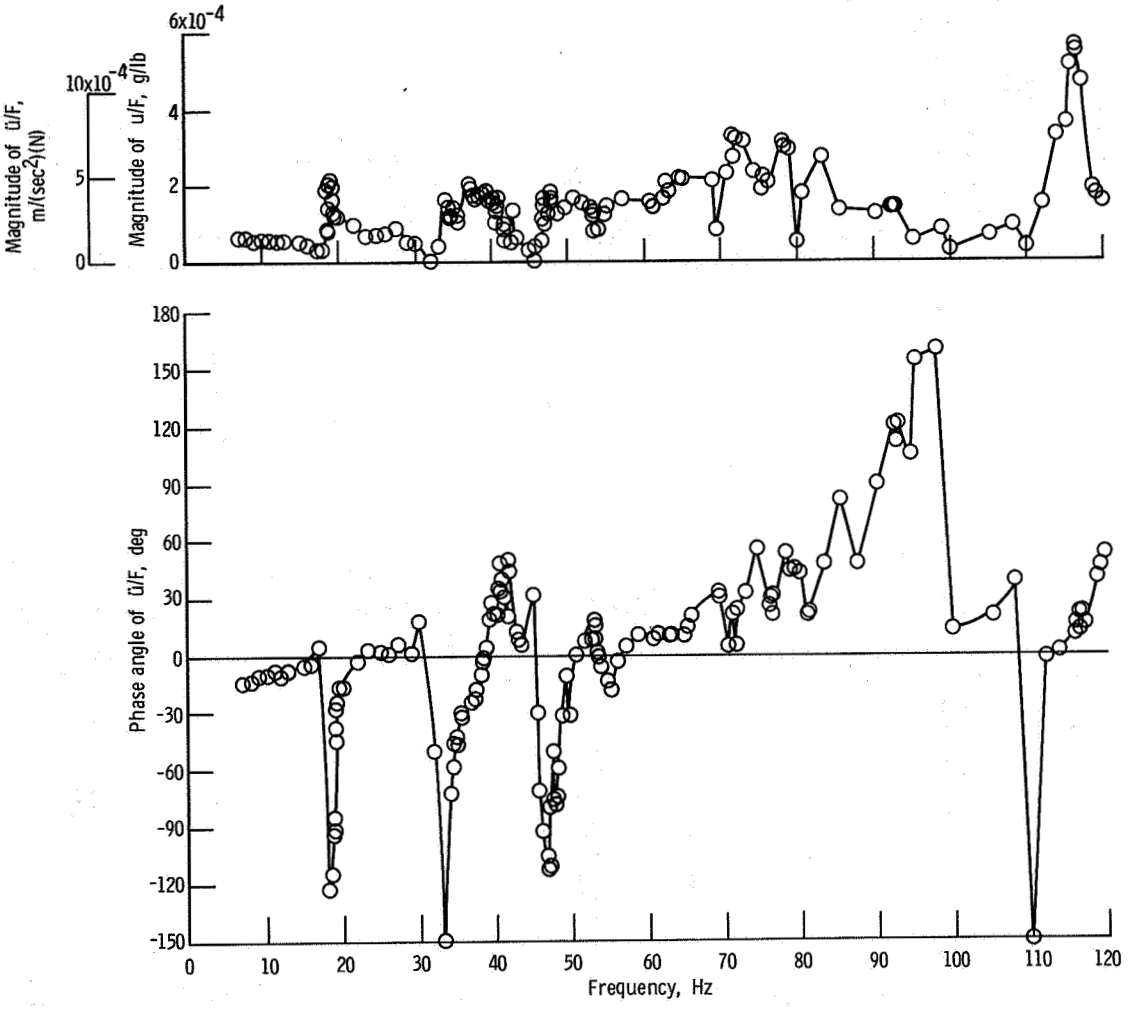

(ℓ) Station 1076.

Figure 10. - Continued.

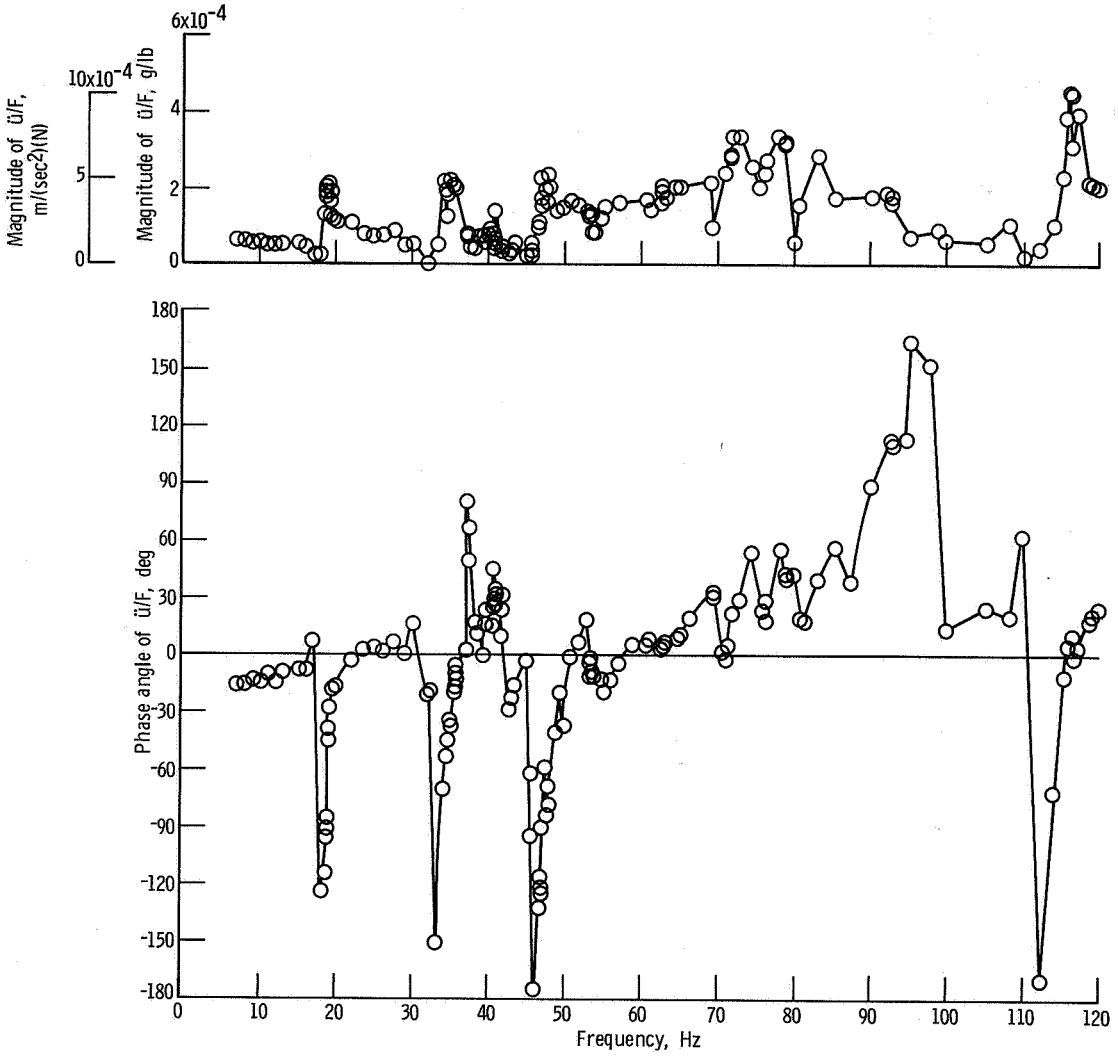

(m) Station 1124.

Figure 10. - Continued.

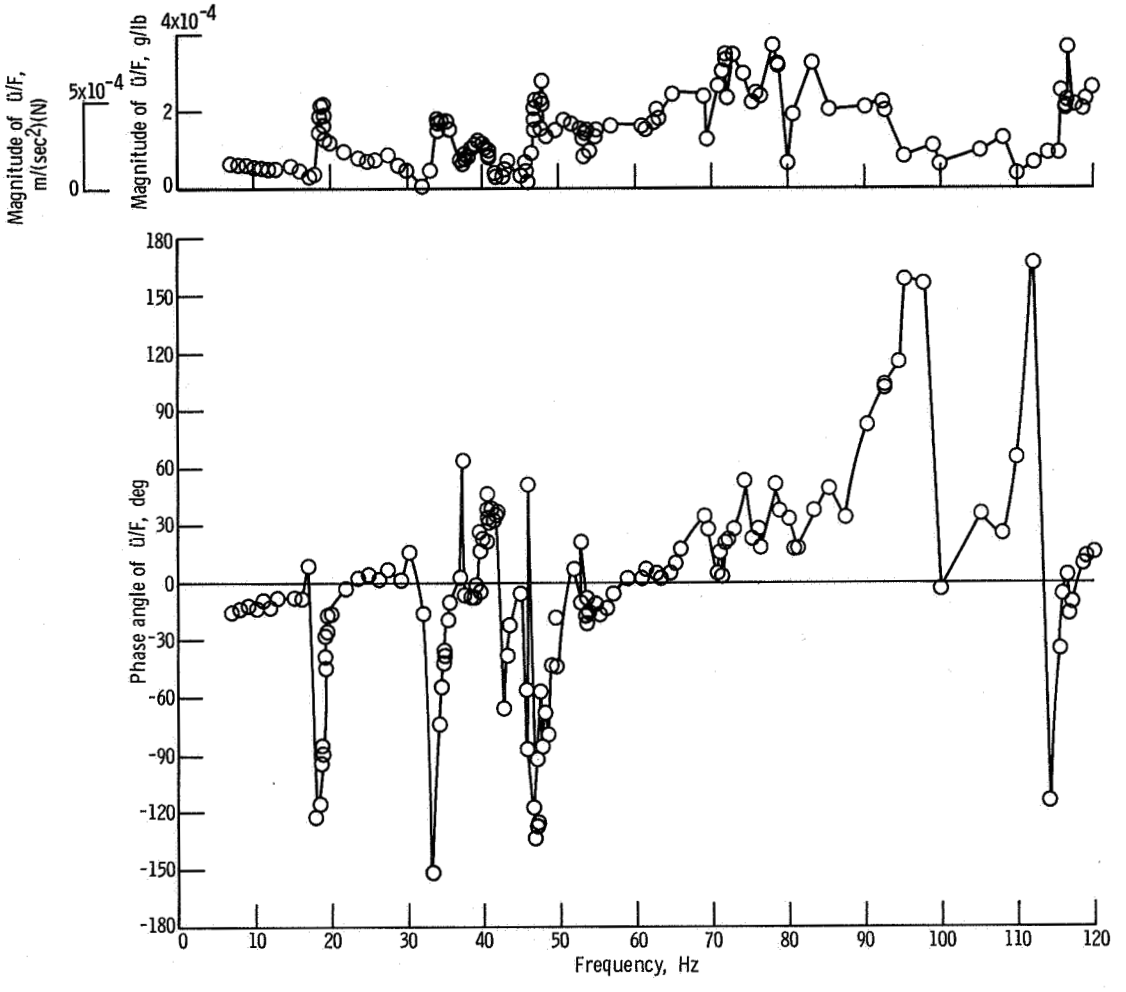

(n) Station 1148.

Figure 10. - Continued.

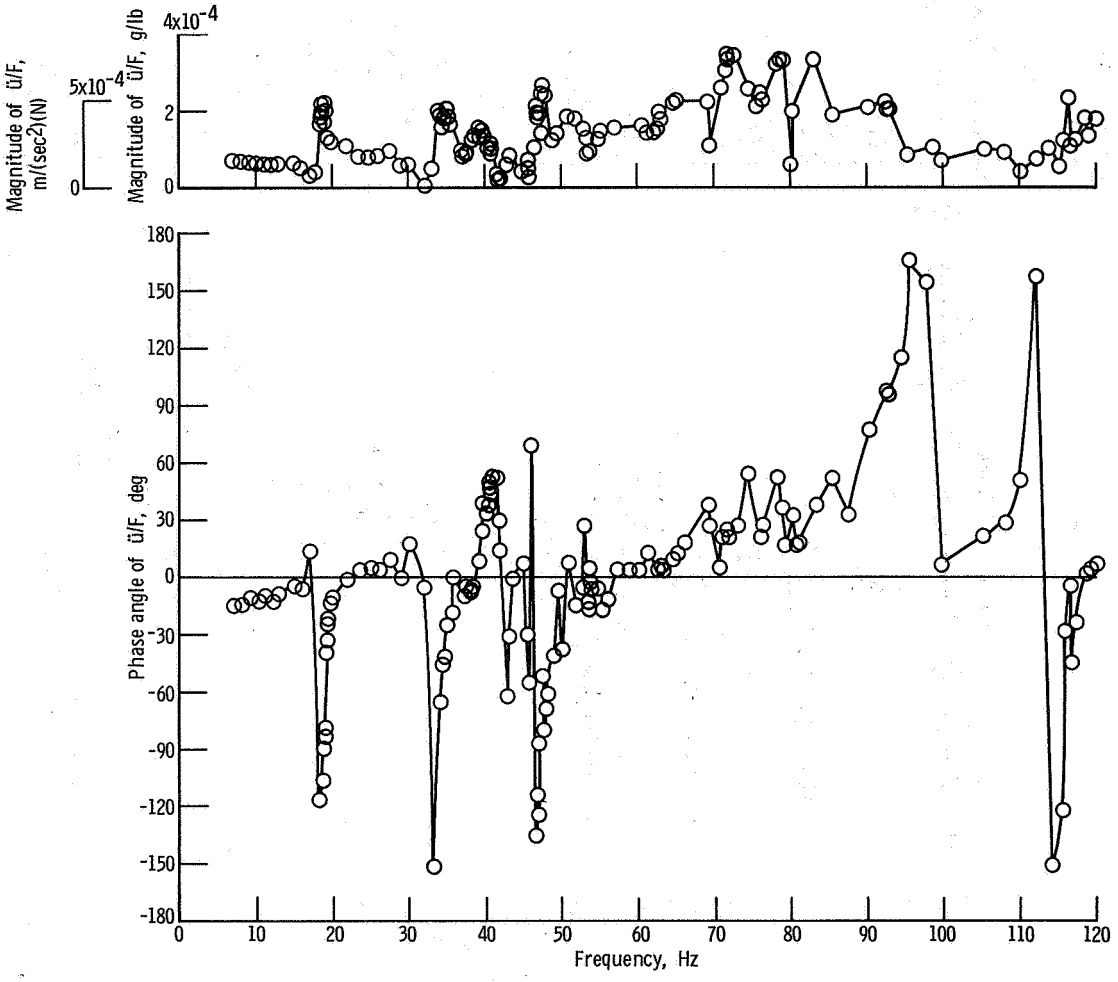

(o) Station 1176.

Figure 10. - Continued.

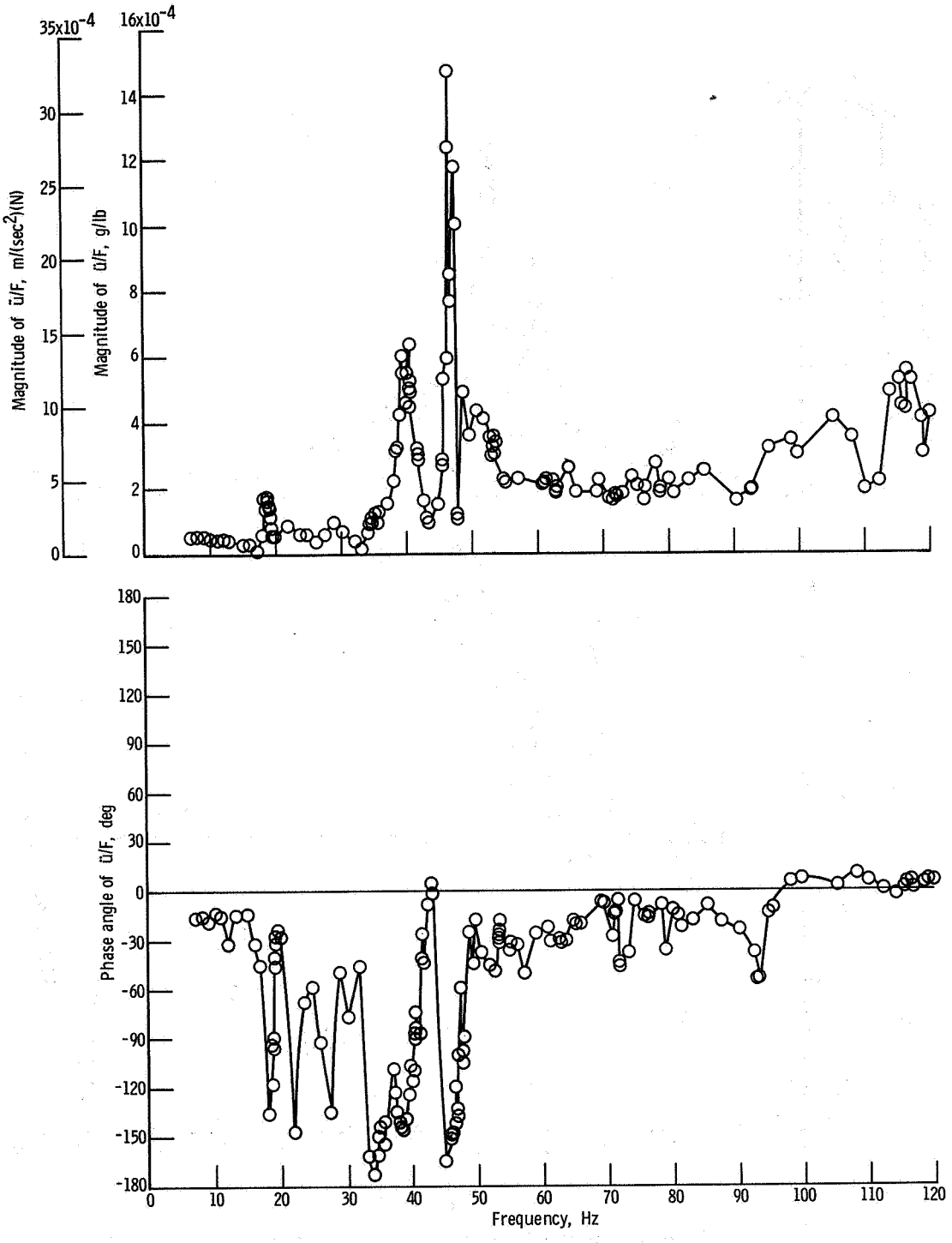

(p) Station 1254.

Figure 10. - Concluded.

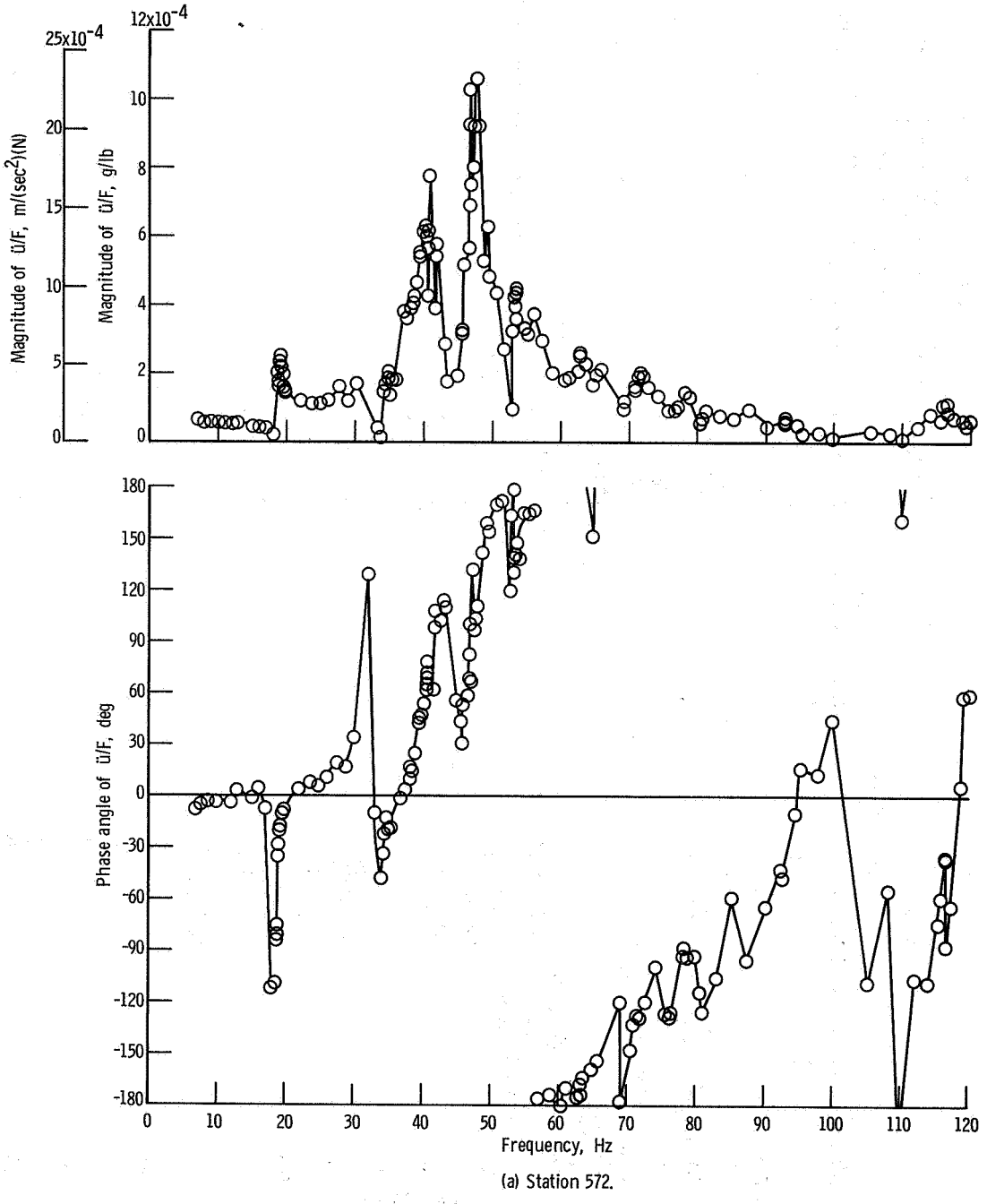

(a) Station 572.

Figure 11. - Longitudinal dynamic response of the vehicle side oriented in the +y-axis direction.

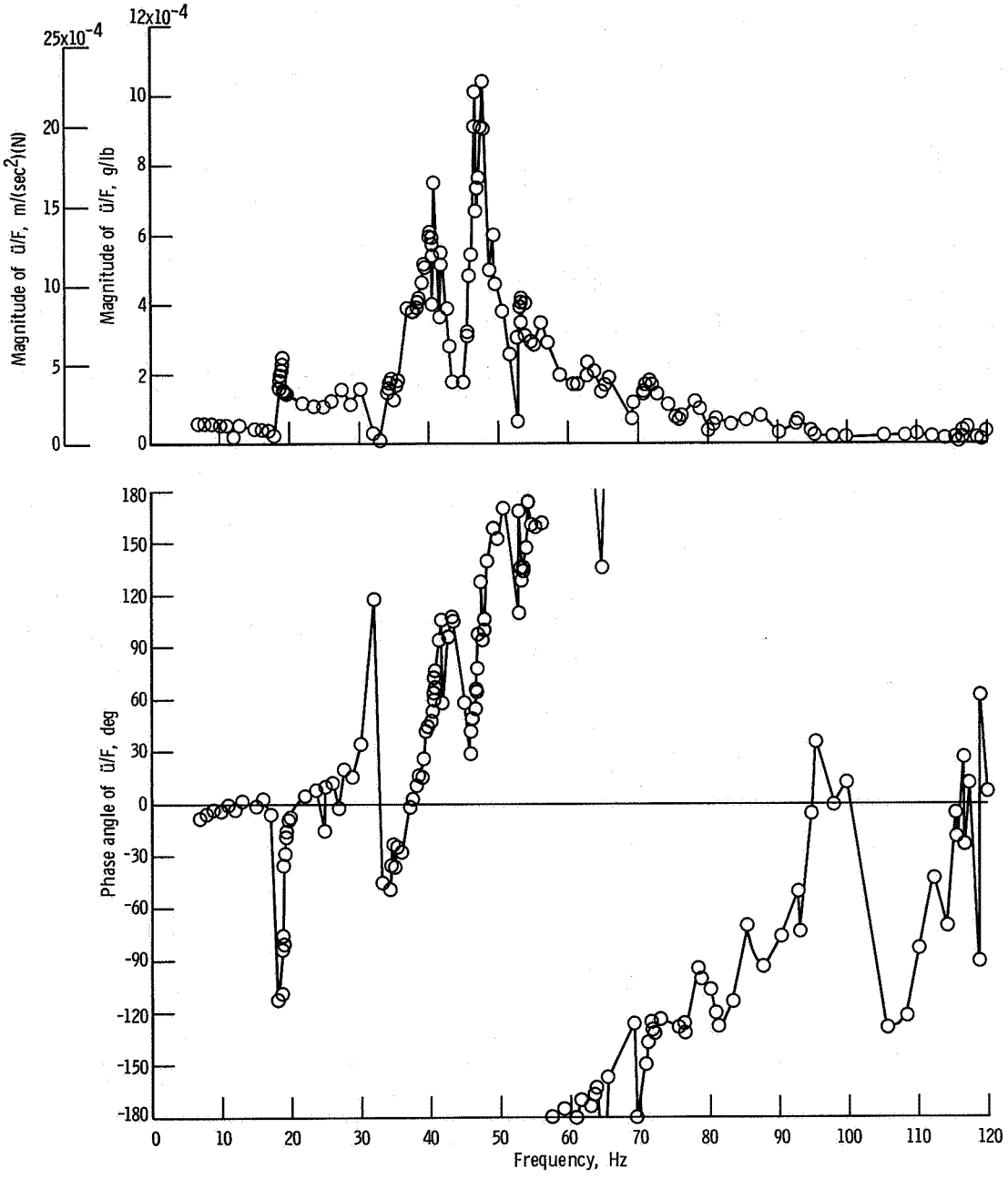

(b) Station 596.

Figure 11. - Continued.

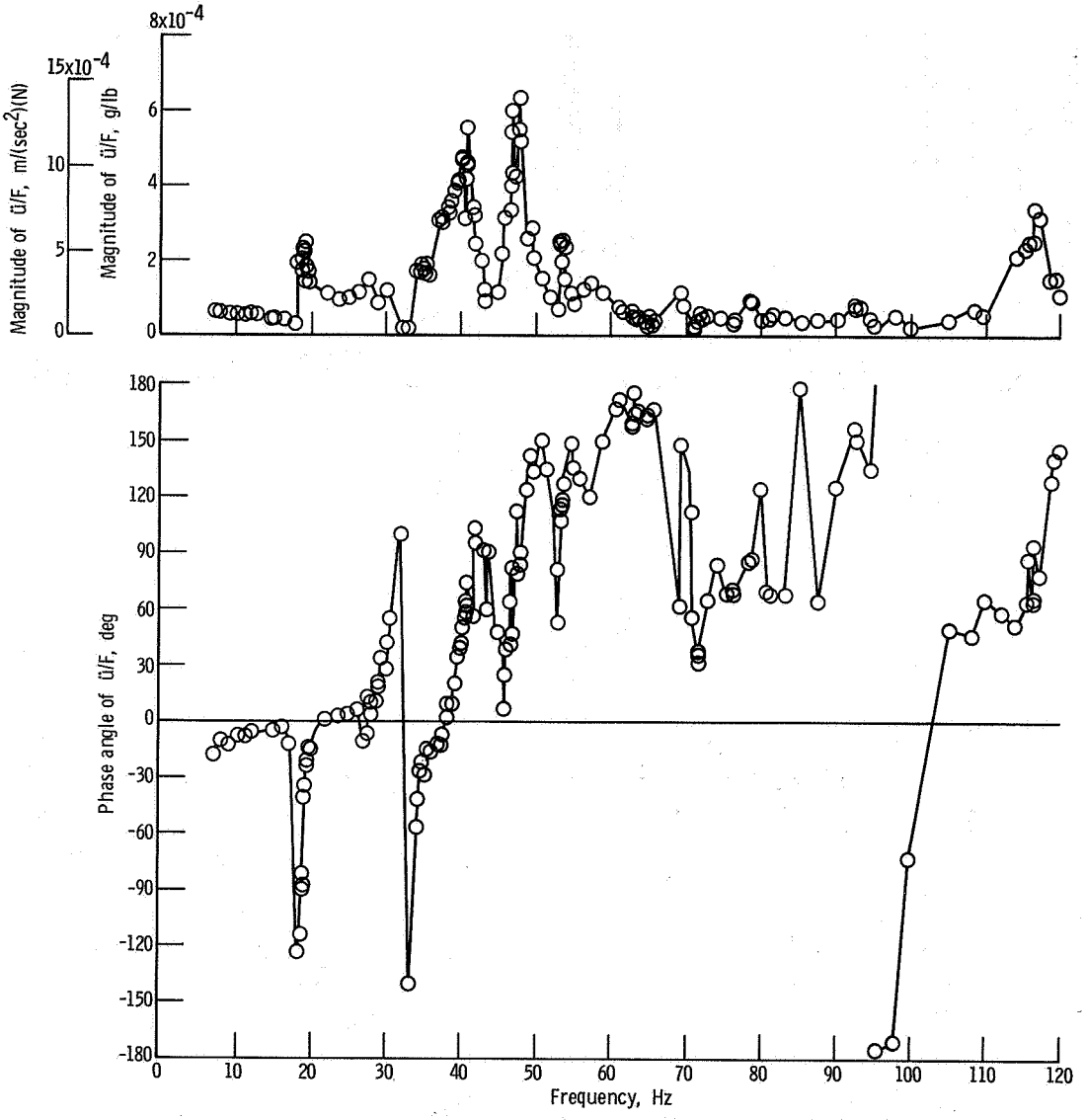

(c) Station 764.

Figure 11. - Continued.

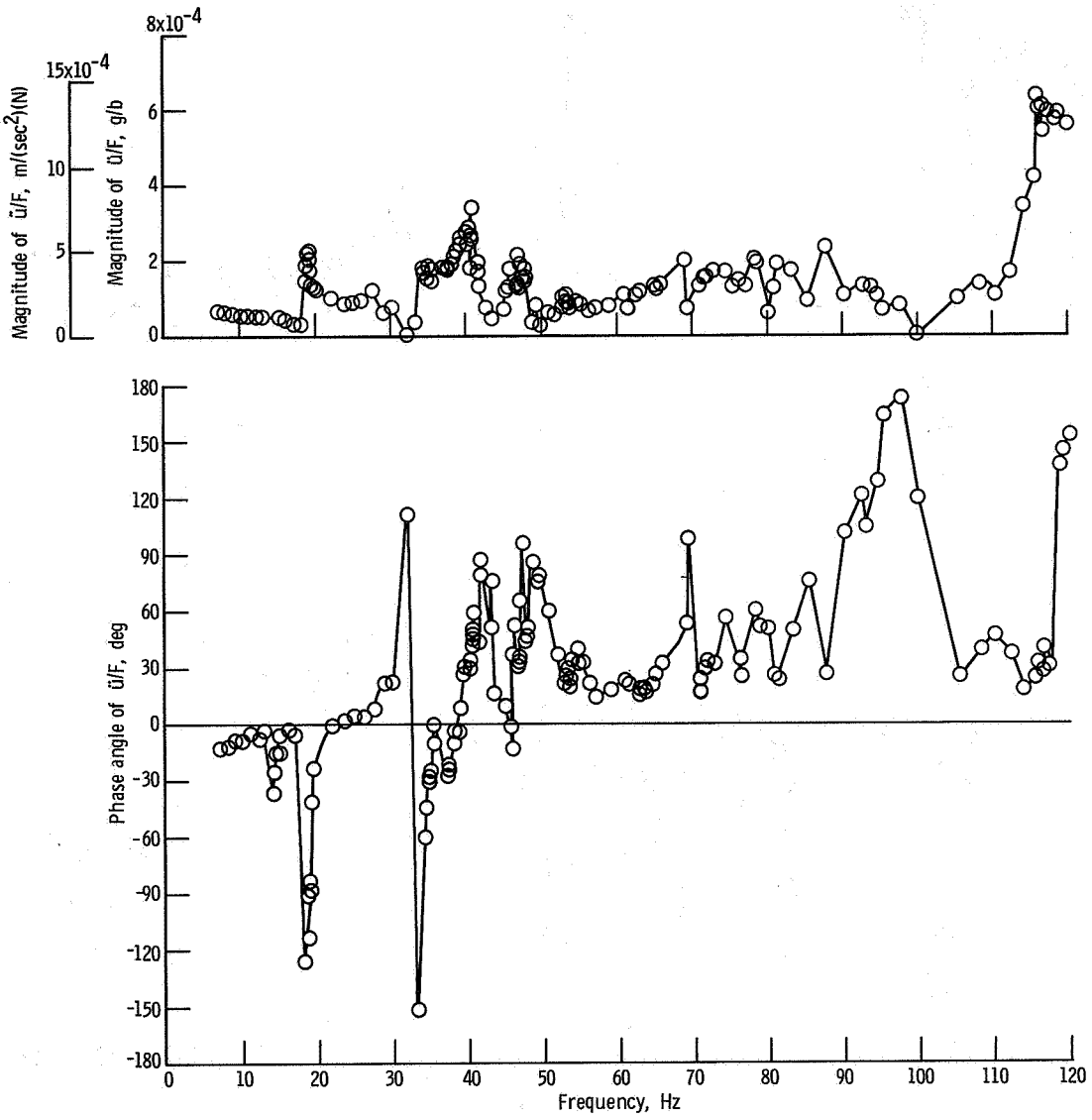

(d) Station 932.

Figure 11. - Continued.

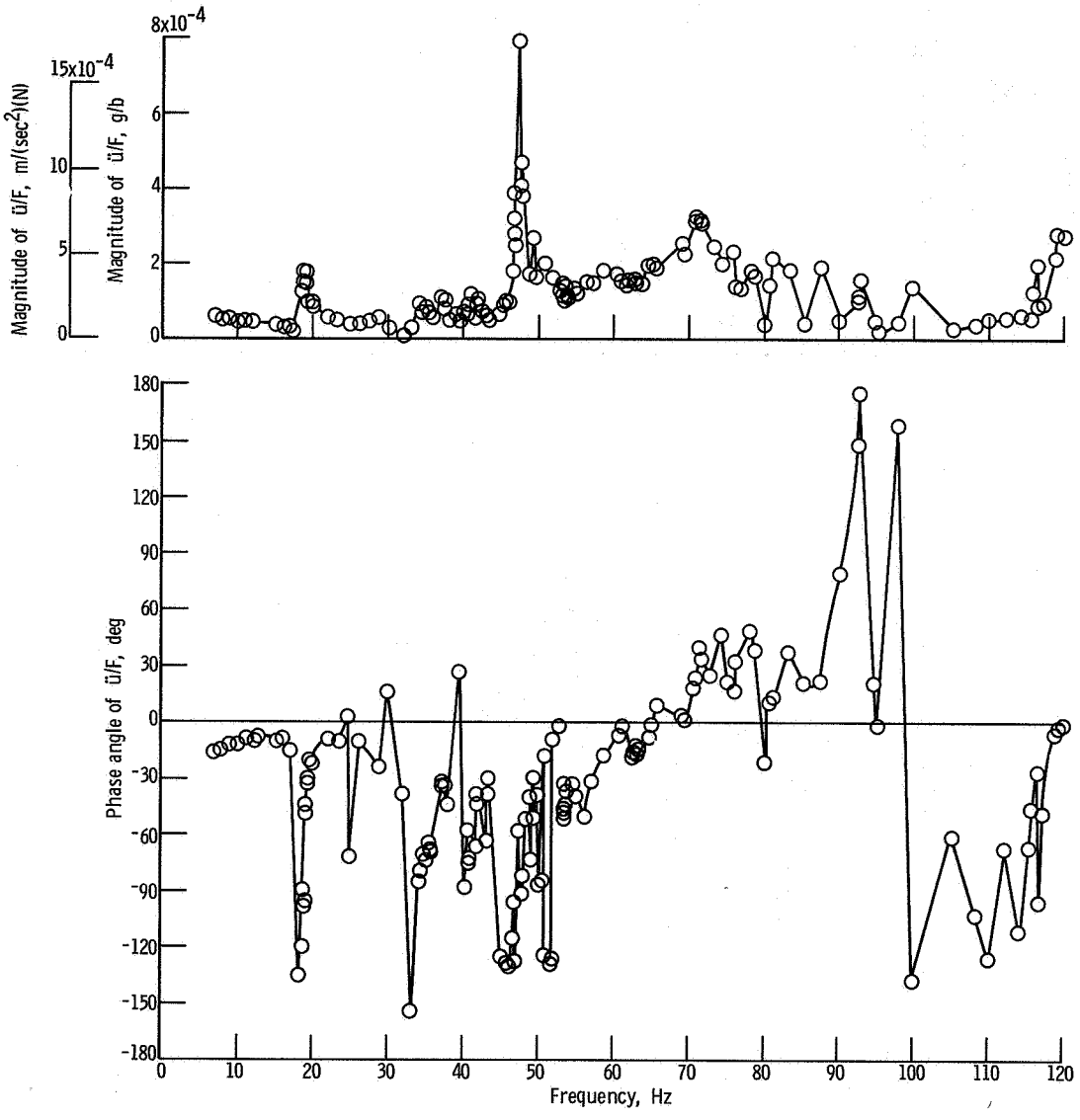

(e) Station 1148.

Figure 11. - Continued.

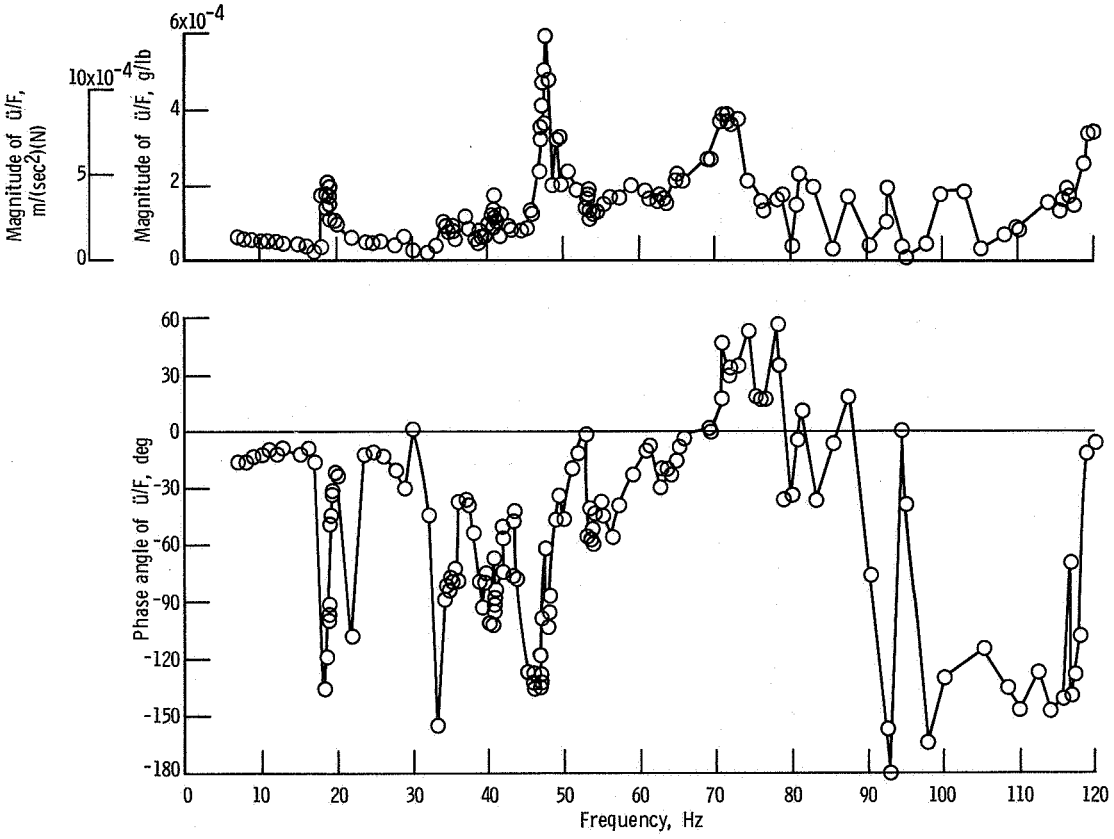

(f) Station 1176.

Figure 11. - Concluded.

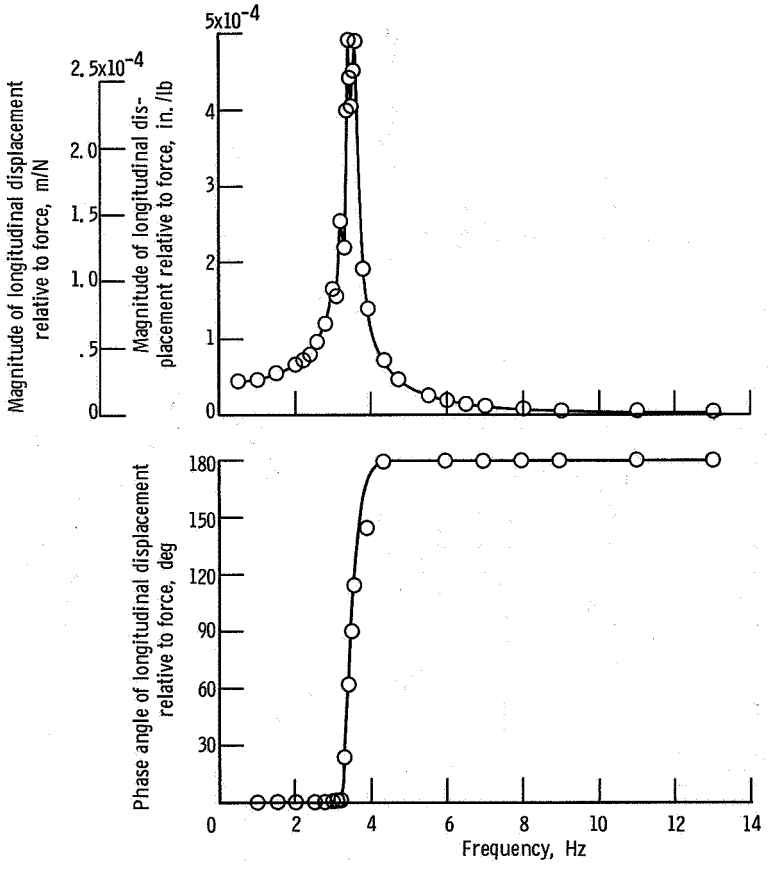

Figure 12. - Longitudinal dynamic response of X-frame.

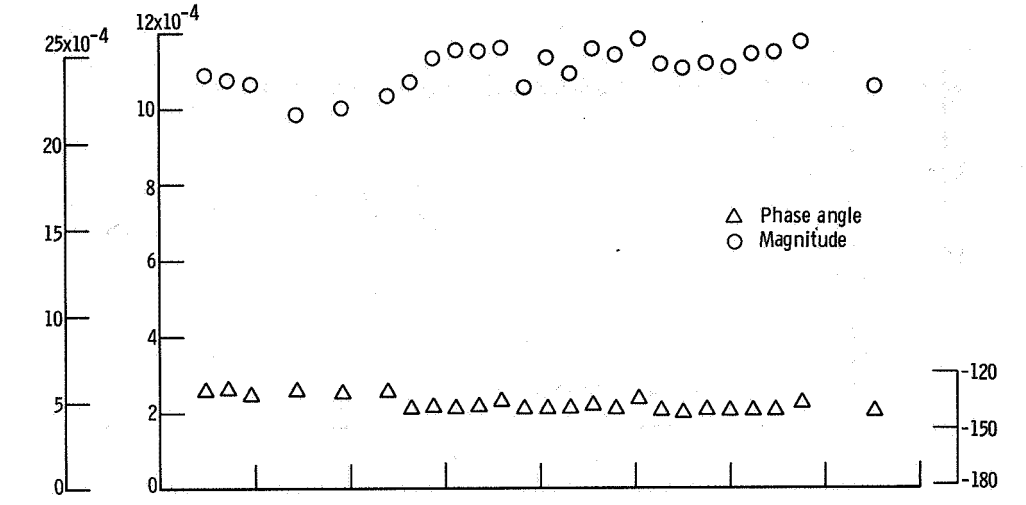

(a) Frequency, 3.4977 hertz.

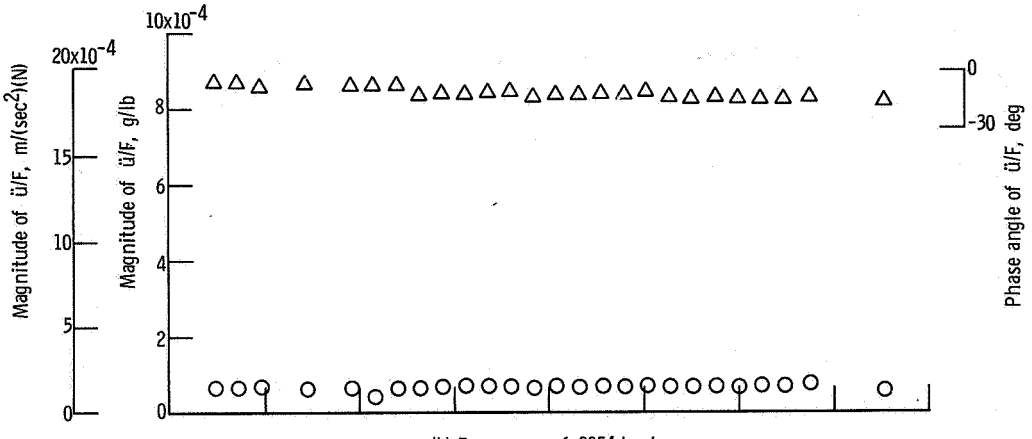

(b) Frequency, 6.9954 hertz.

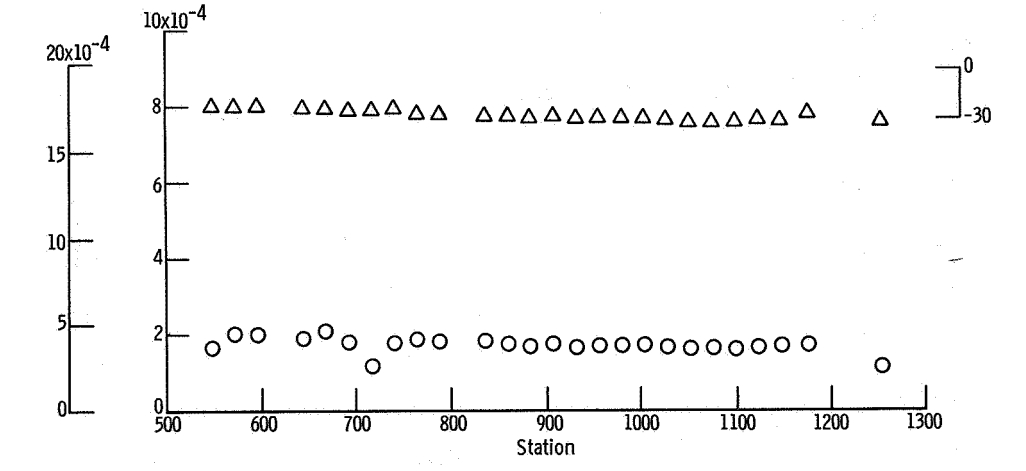

(c) Frequency, 19.206 hertz.

Figure 13. - Vehicle dynamic shape at a given frequency.

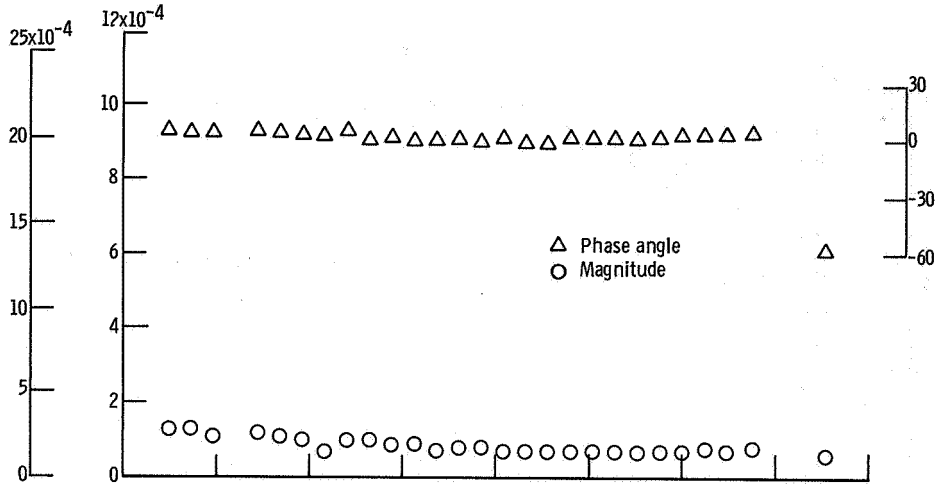

(d) Frequency, 24.944 hertz.

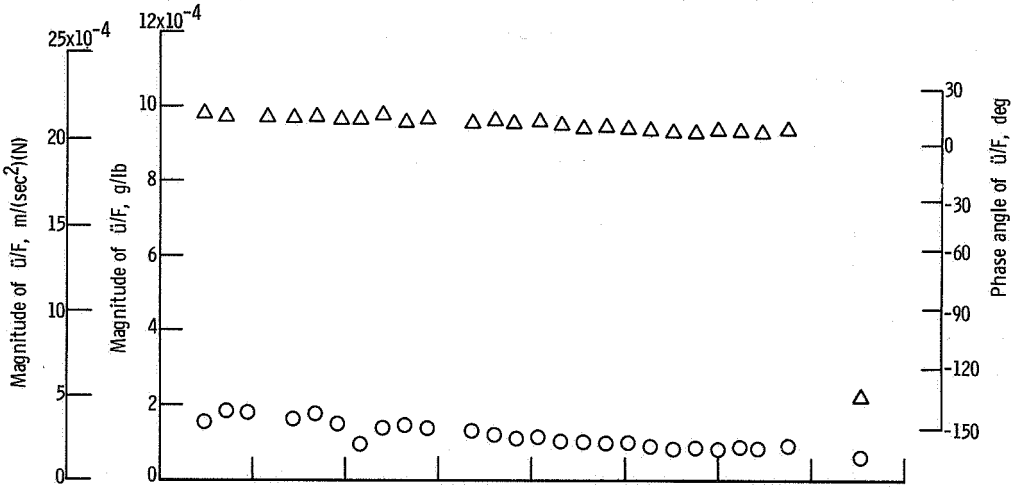

(e) Frequency, 27.537 hertz.

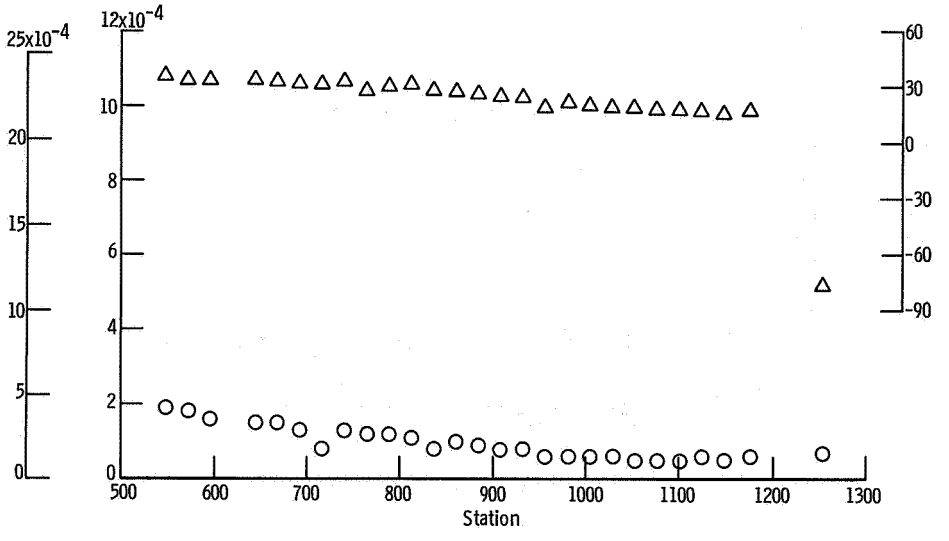

(f) Frequency, 30.141 hertz.

Figure 13. - Continued.

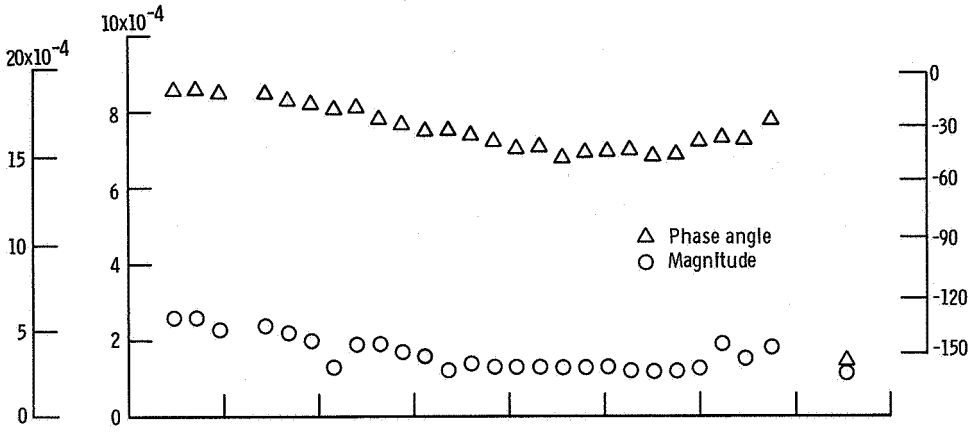

(g) Frequency, 34.877 hertz.

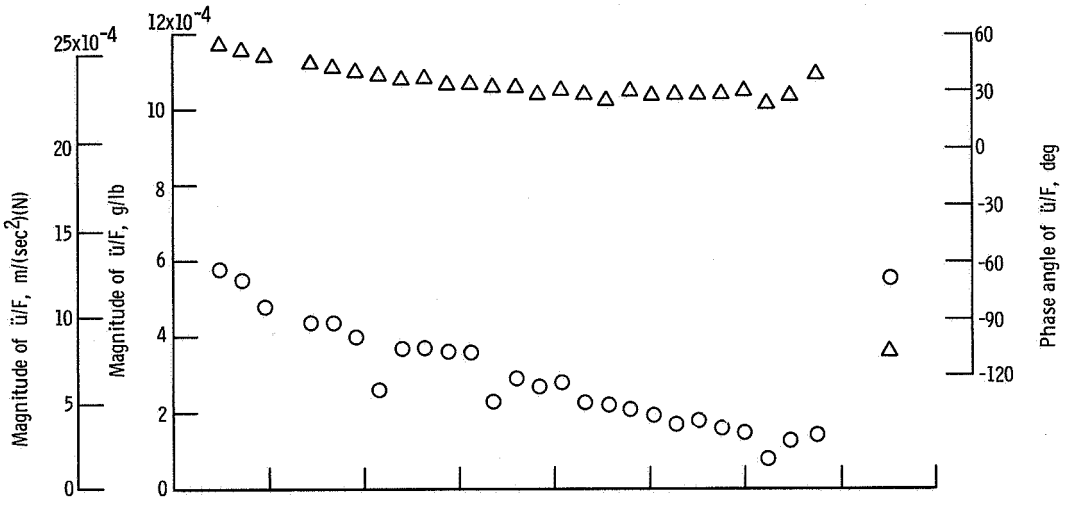

(h) Frequency, 39.617 hertz.

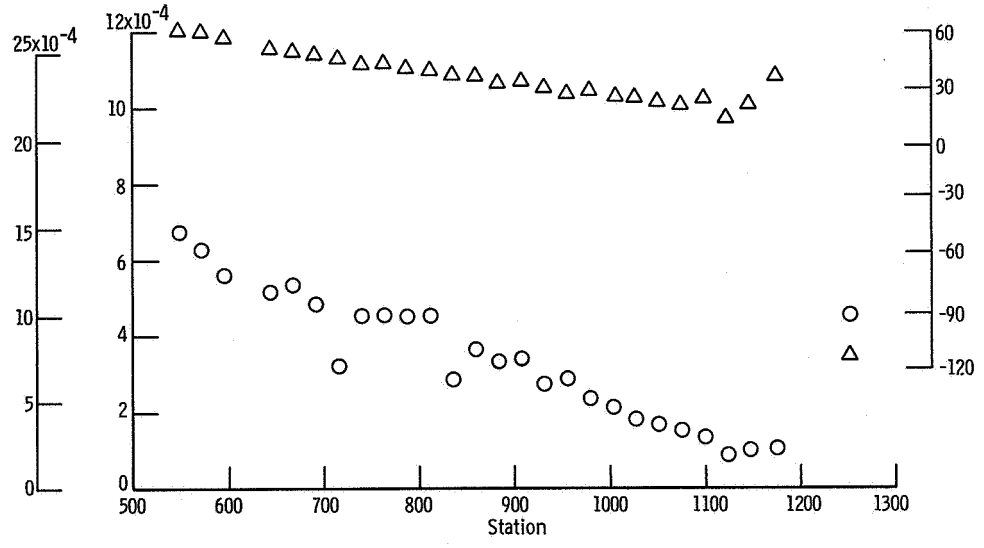

(i) Frequency, 40.354 hertz.

Figure 13. - Continued.

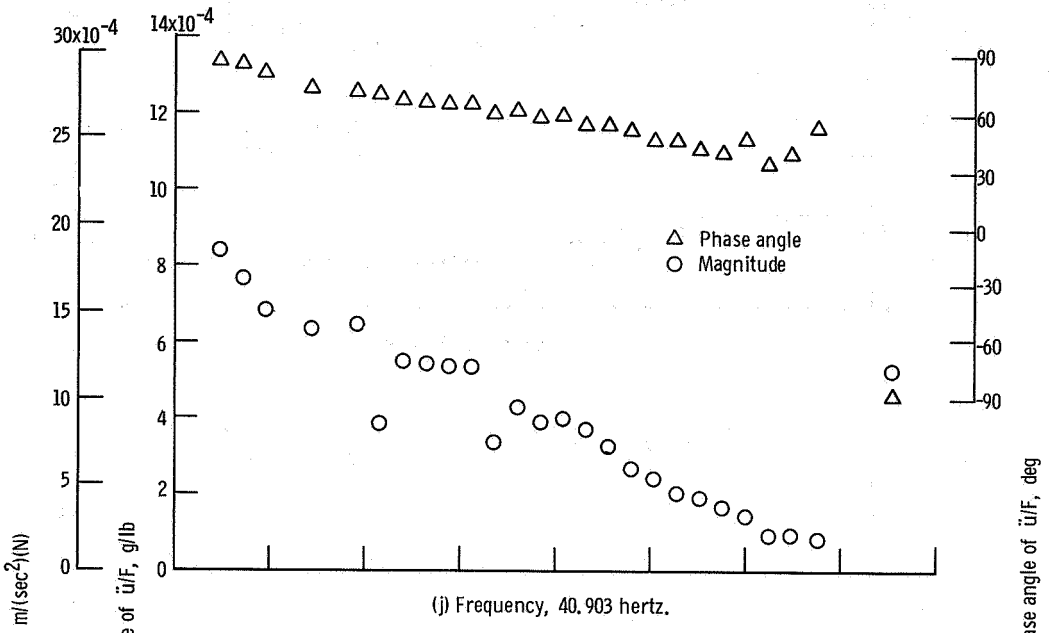

(j) Frequency, 40.903 hertz.

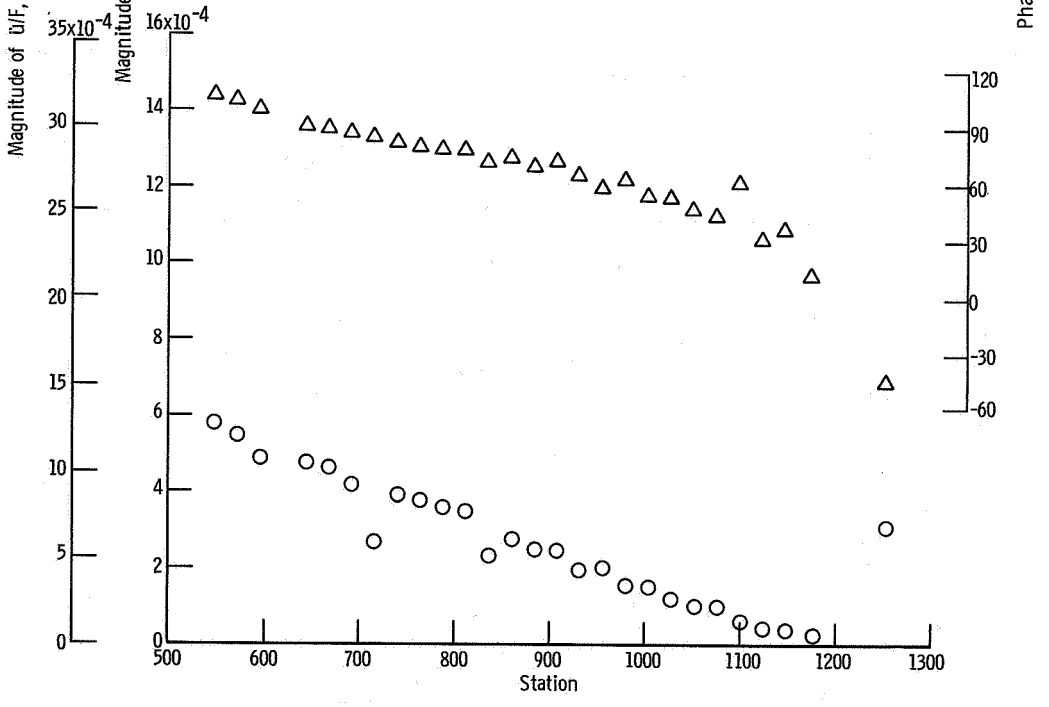

(k) Frequency, 41.823 hertz.

Figure 13. - Continued.

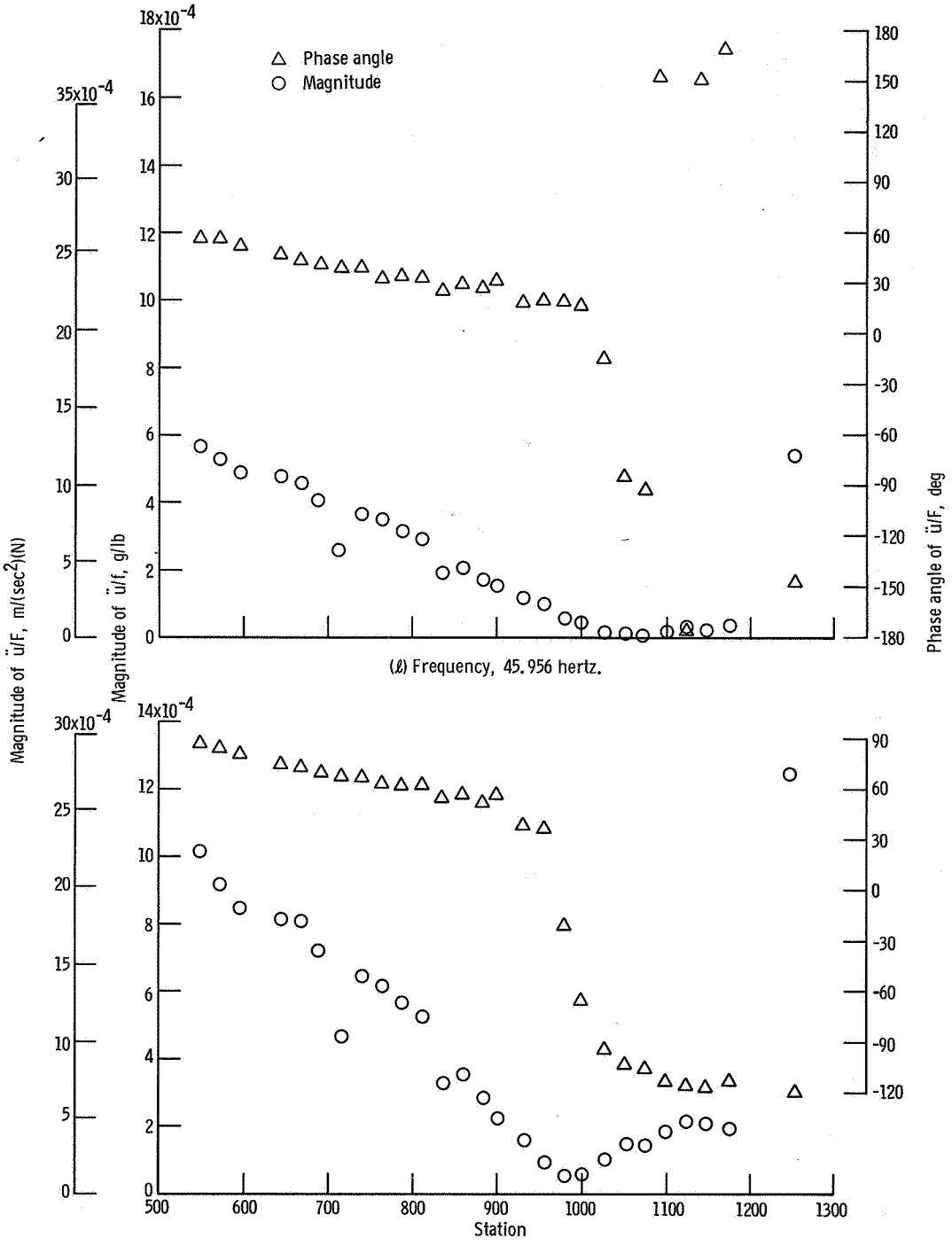

(ℓ) Frequency, 45.956 hertz.

(m) Frequency, 46.725 hertz.

Figure 13. - Continued.

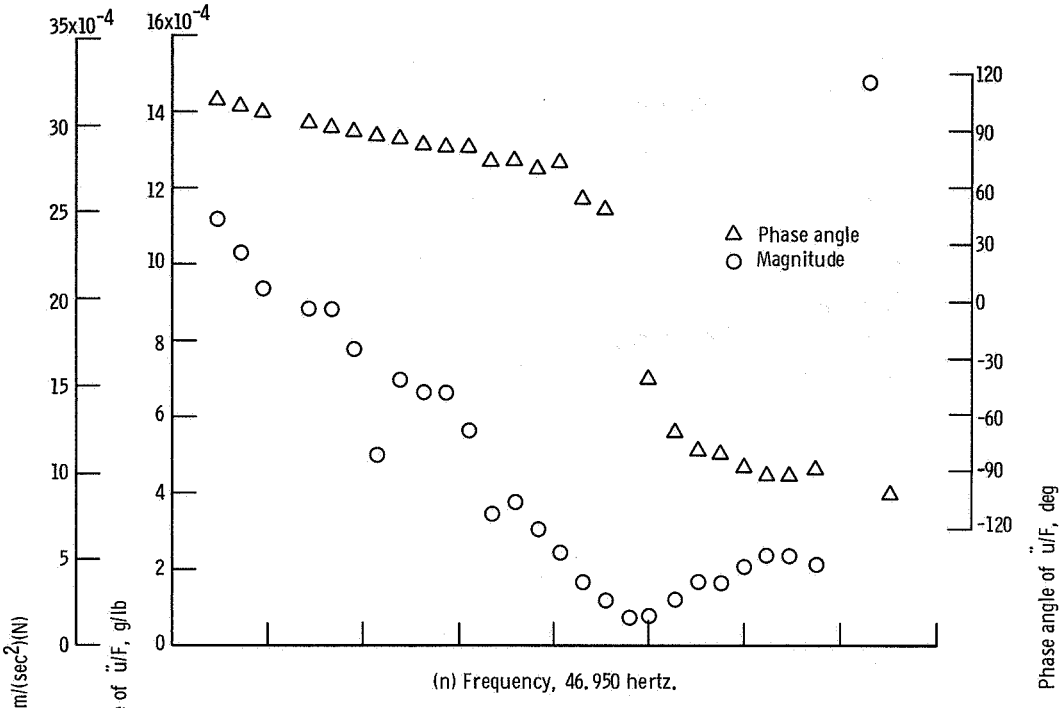

(n) Frequency, 46.950 hertz.

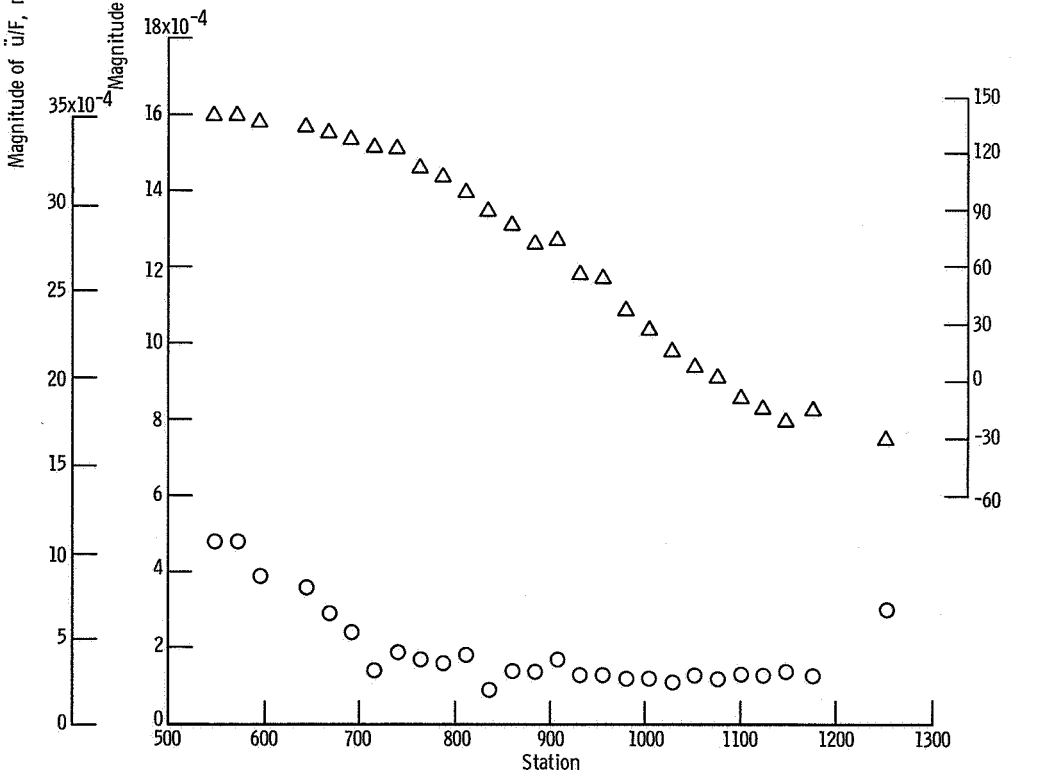

(o) Frequency, 53.437 hertz.

Figure 13. - Continued.

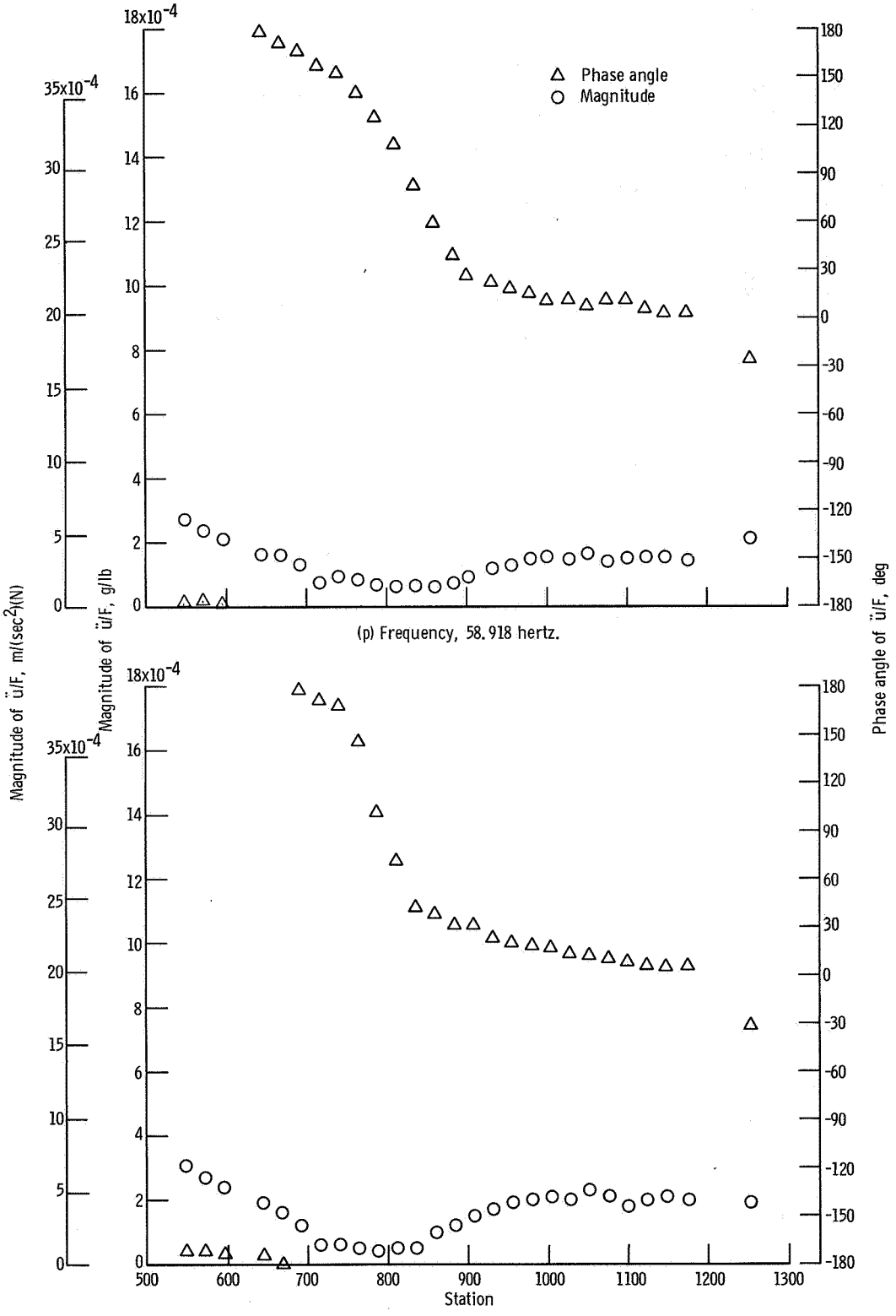

(p) Frequency, 58.918 hertz.

(q) Frequency, 62.903 hertz.

Figure 13. - Continued.

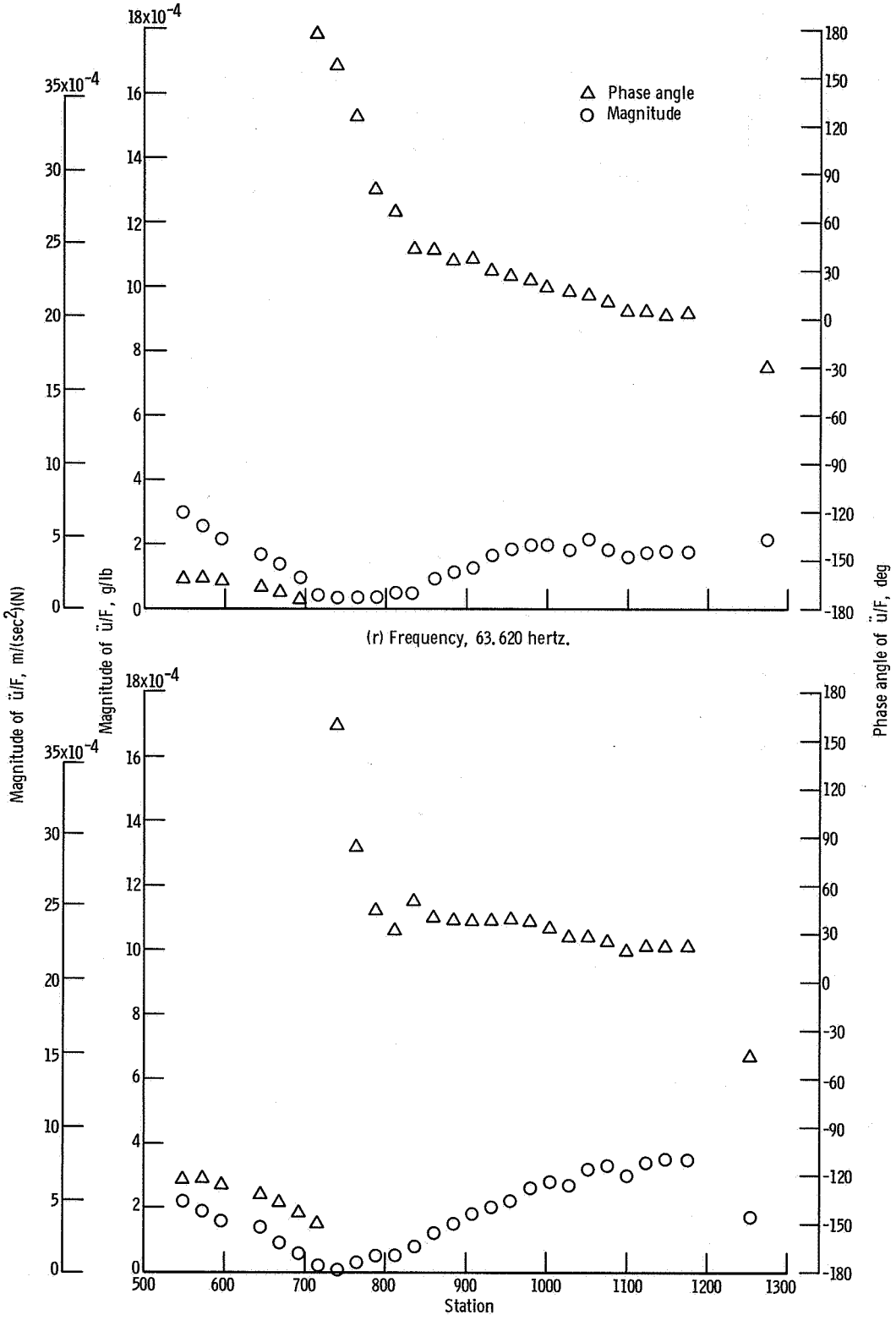

(r) Frequency, 63.620 hertz.

(s) Frequency, 71.803 hertz.

Figure 13. - Continued.

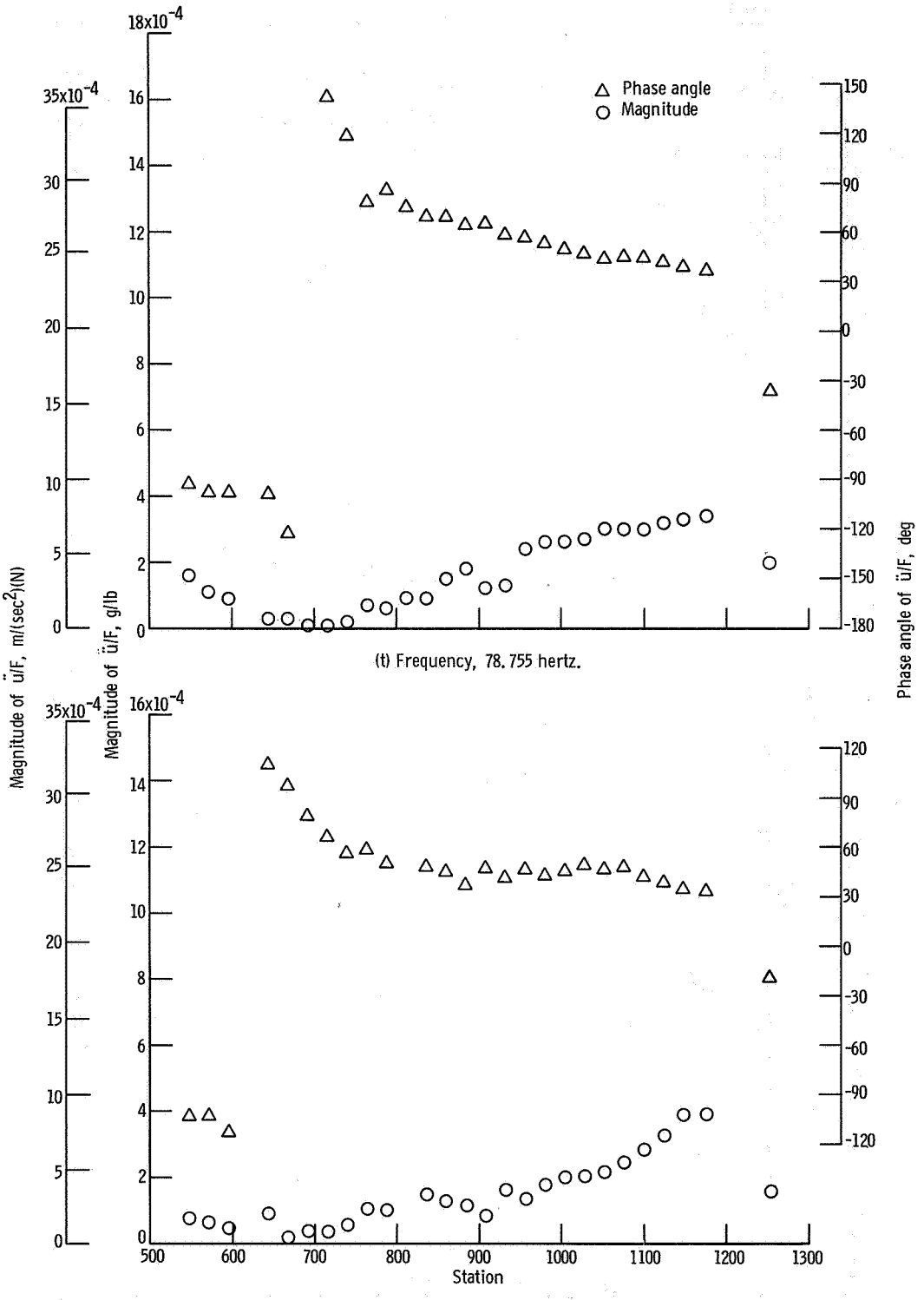

(t) Frequency, 78.755 hertz.

(u) Frequency, 87.54 hertz.

Figure 13. - Continued.

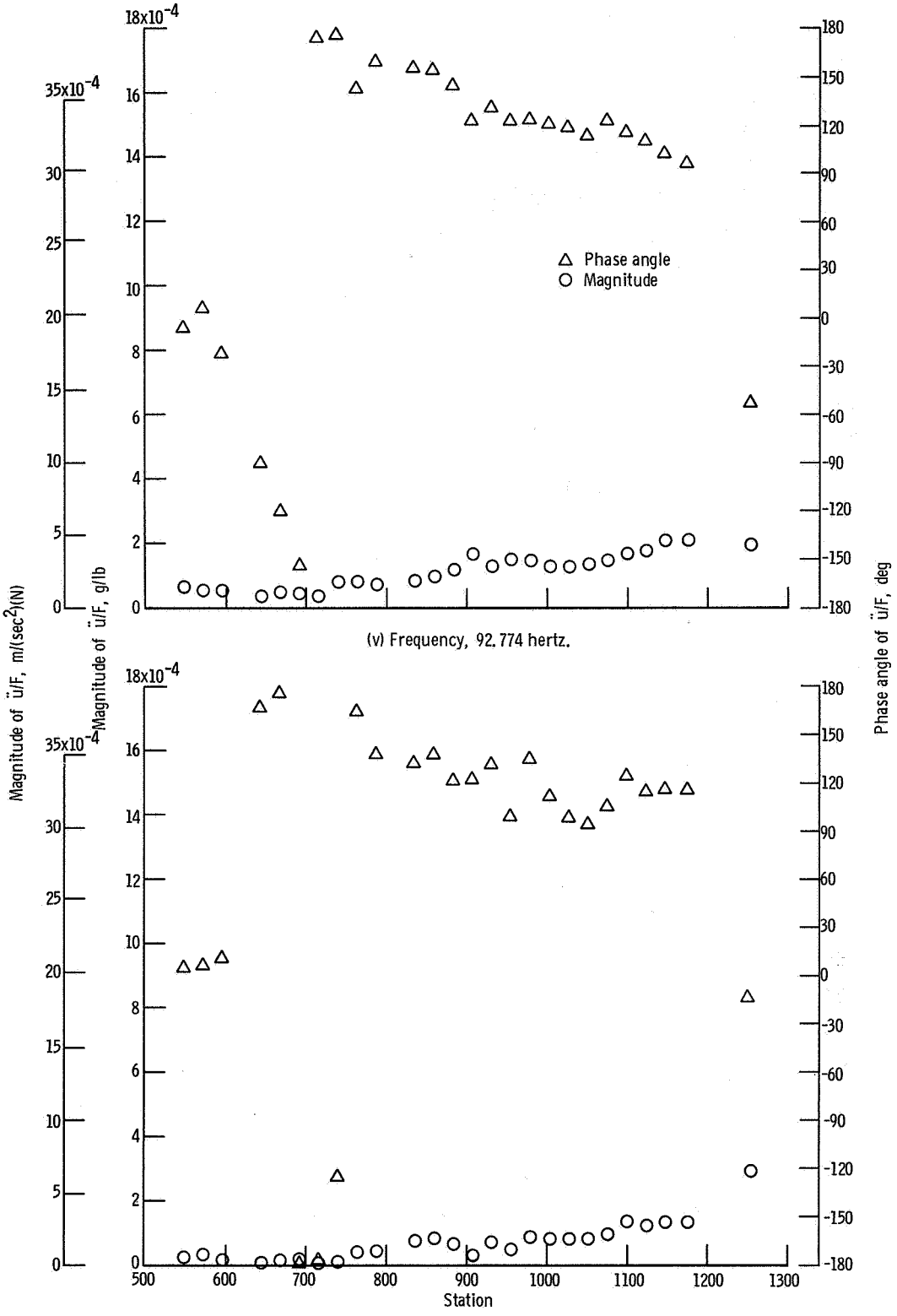

(v) Frequency, 92.774 hertz.

(w) Frequency, 94.663 hertz.

Figure 13. - Continued.

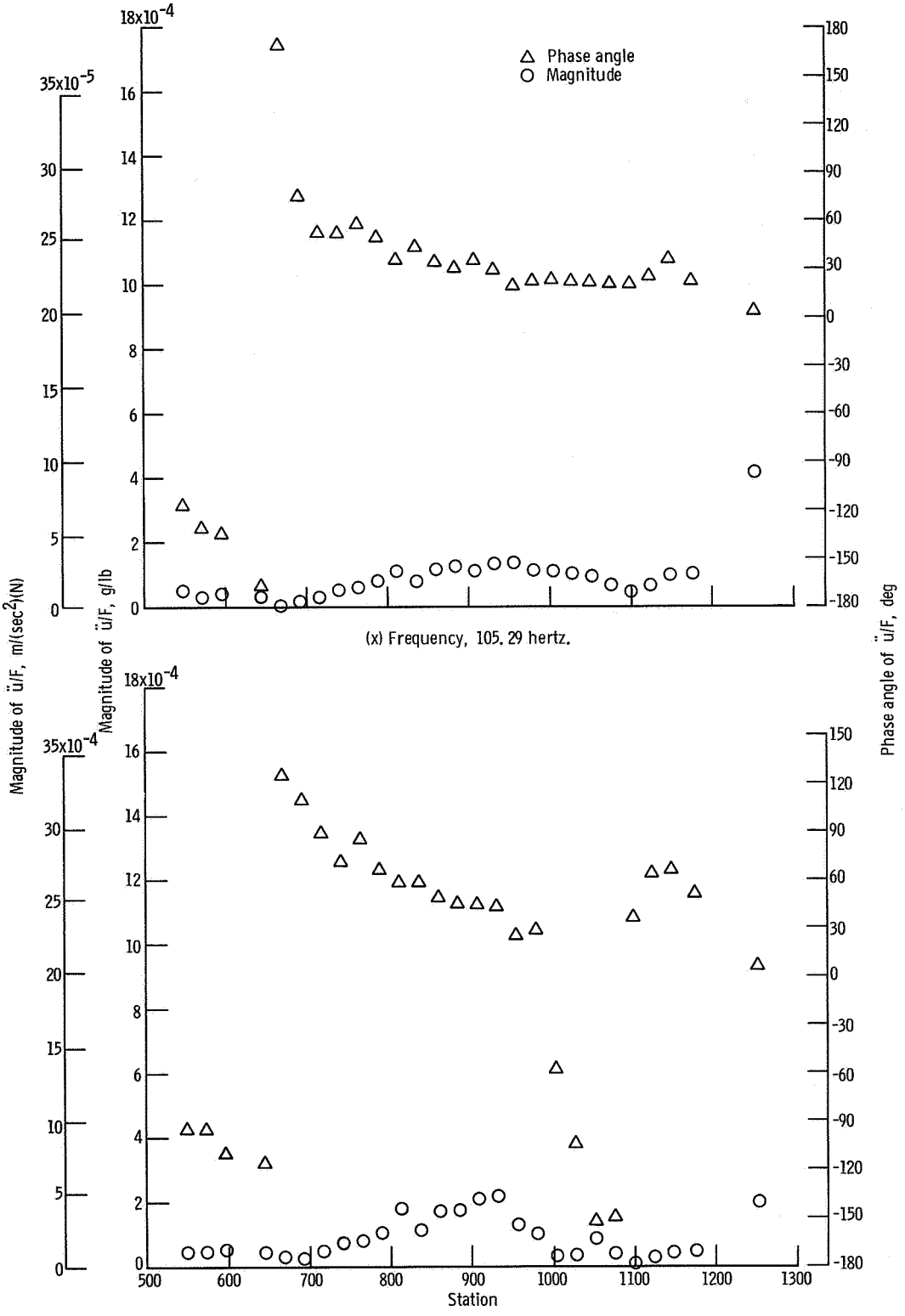

(x) Frequency, 105.29 hertz.

(y) Frequency, 110.04 hertz.

Figure 13. - Continued.

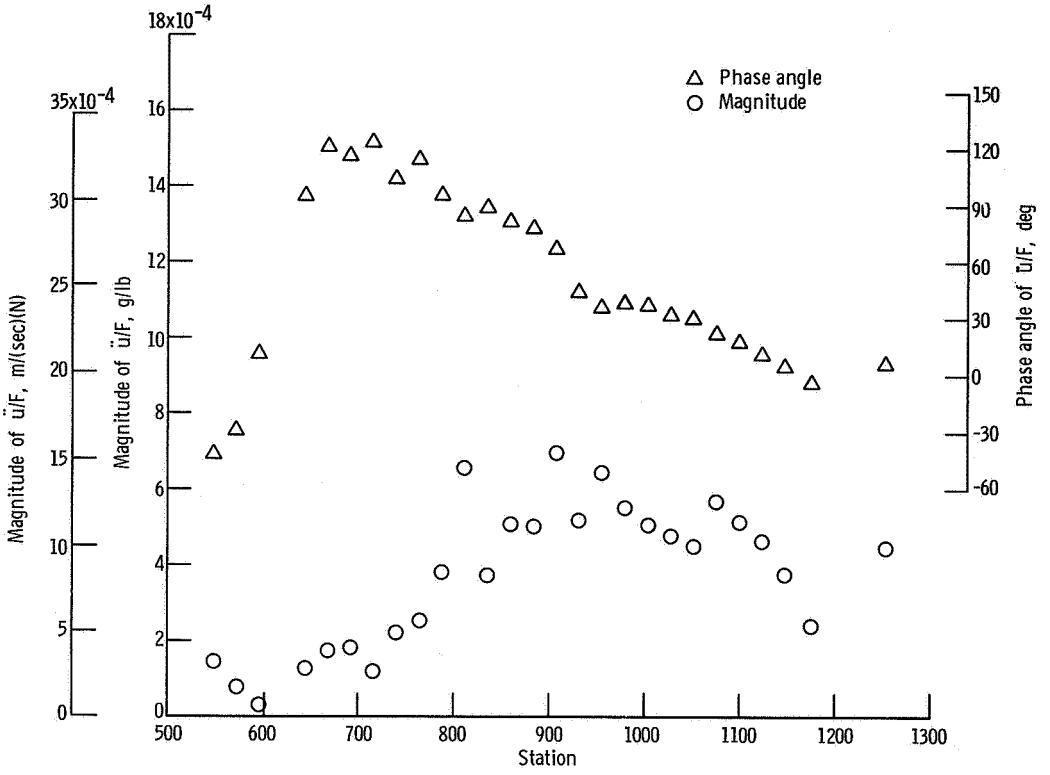

(z) Frequency, 116.60 hertz.

Figure 13. - Concluded.

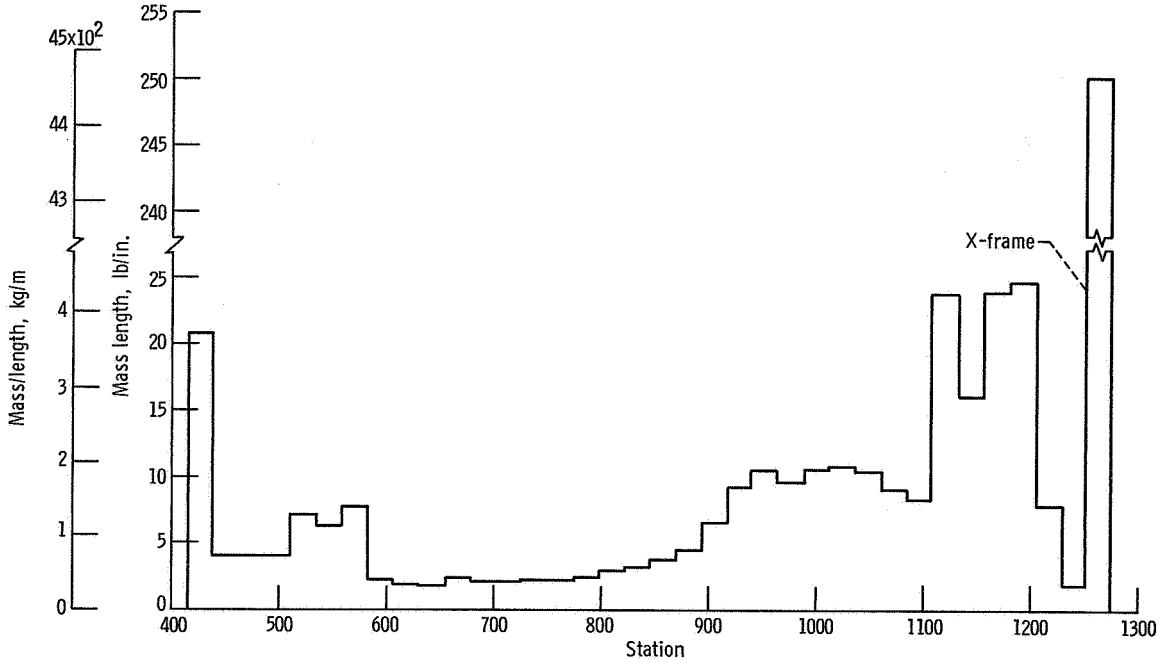

Figure 14. - Vehicle mass distribution.

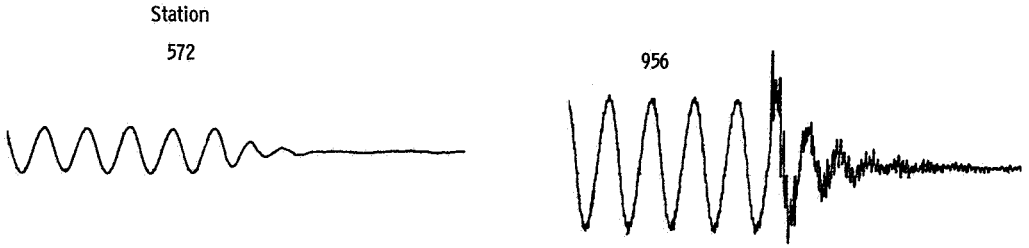

(a) Frequency, 3.5 hertz; damping ratio, 0.05.

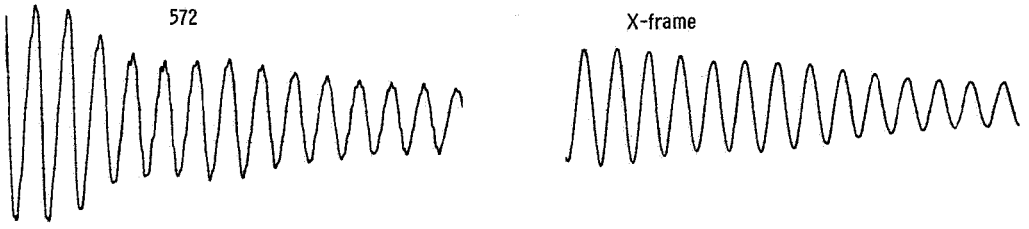

(b) Frequency, 47 hertz; damping ratio, 0.016.

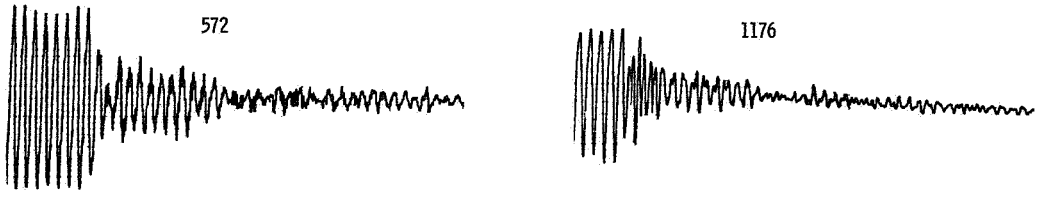

(c) Frequency, 72 hertz; damping ratio, 0.0145.

Figure 15. - Typical transient data used for logarithmic decay determination of damping ratio.

"The aeronautical and space activities of the United States shall be conducted so as to contribute . . . to the expansion of human knowledge of phenomena in the atmosphere and space. The Administration shall provide for the widest practicable and appropriate dissemination of information concerning its activities and the results thereof."

—NATIONAL AERONAUTICS AND SPACE ACT OF 1958

NASA SCIENTIFIC AND TECHNICAL PUBLICATIONS

TECHNICAL REPORTS: Scientific and technical information considered important, complete, and a lasting contribution to existing knowledge.

TECHNICAL NOTES: Information less broad in scope but nevertheless of importance as a contribution to existing knowledge.

TECHNICAL MEMORANDUMS: Information receiving limited distribution because of preliminary data, security classification, or other reasons.

CONTRACTOR REPORTS: Scientific and technical information generated under a NASA contract or grant and considered an important contribution to existing knowledge.

TECHNICAL TRANSLATIONS: Information published in a foreign language considered to merit NASA distribution in English.

SPECIAL PUBLICATIONS: Information derived from or of value to NASA activities. Publications include conference proceedings, monographs, data compilations, handbooks, sourcebooks, and special bibliographies.

TECHNOLOGY UTILIZATION PUBLICATIONS: Information on technology used by NASA that may be of particular interest in commercial and other non-aerospace applications. Publications include Tech Briefs, Technology Utilization Reports and Notes, and Technology Surveys.

Details on the availability of these publications may be obtained from:

SCIENTIFIC AND TECHNICAL INFORMATION DIVISION

NATIONAL AERONAUTICS AND SPACE ADMINISTRATION

Washington, D.C. 20546